arXiv:1601.02775v2 [stat.AP] 20 Jun 2016

Separating timing, movement conditions and individual differences in the analysis of human movement

LARS LAU RAKET[1], BRITTA GRIMME[2], GREGOR SCHÖNER[2], CHRISTIAN IGEL[3], and BO MARKUSSEN[1]

[1] *Department of Mathematical Sciences, University of Copenhagen, Universitetsparken 5, 2100 Copenhagen, Denmark.*

[2] *Institut für Neuroinformatik, Ruhr-Universität Bochum, Universitätsstraße 150, D-44801 Bochum, Germany.*

[3] *Department of Computer Science, University of Copenhagen, Sigurdsgade 41 2200 Copenhagen, Denmark.*

Abstract: A central task in the analysis of human movement behavior is to determine systematic patterns and differences across experimental conditions, participants and repetitions. This is possible because human movement is highly regular, being constrained by invariance principles. Movement timing and movement path, in particular, are linked through scaling laws. Separating variations of movement timing from the spatial variations of movements is a well-known challenge that is addressed in current approaches only through forms of preprocessing that bias analysis. Here we propose a novel nonlinear mixed-effects model for analyzing temporally continuous signals that contain systematic effects in both timing and path. Identifiability issues of path relative to timing are overcome by using maximum likelihood estimation in which the most likely separation of space and time is chosen given the variation found in data. The model is applied to analyze experimental data of human arm movements in which participants move a hand-held object to a target location while avoiding an obstacle. The model is used to classify movement data according to participant. Comparison to alternative approaches establishes nonlinear mixed-effects models as viable alternatives to conventional analysis frameworks. The model is then combined with a novel factor-analysis model that estimates the low-dimensional subspace within which movements vary when the task demands vary. Our framework enables us to visualize different dimensions of movement variation and to test hypotheses about the effect of obstacle placement and height on the movement path. We demonstrate that the approach can be used to uncover new properties of human movement.

Author Summary

When you move a cup to a new location on a table, the movement of lifting, transporting, and setting down the cup appears to be completely automatic. Although the hand could take continuously many different paths and move on any temporal trajectory, real movements are highly regular and reproducible. From repetition to repetition movemens vary, and the pattern of variance reflects movement conditions and movement timing. If another person performs the same task, the movement will be similar. When we look more closely, however, there are systematic individual differences. Some people will overcompensate when avoiding an obstacle and some people will systematically move slower than others. When we want to understand human movement, all these aspects are important. We want to know which parts of a movement are common across people and we want to quantify the different types of variability. Thus, the models we use to analyze movement data should contain all the mentioned effects. In this work, we developed a framework for statistical analysis of movement data that respects these structures of movements. We showed how this framework modeled the individual characteristics of participants better than other state-of-the-art modeling approaches. We

combined the timing-and-path-separating model with a novel factor analysis model for analyzing the effect of obstacles on spatial movement paths. This combination allowed for an unprecedented ability to quantify and display different sources of variation in the data. We analyzed data from a designed experiment of arm movements under various obstacle avoidance conditions. Using the proposed statistical models, we documented three findings: a linearly amplified deviation in mean path related to increase in obstacle height; a consistent asymmetric pattern of variation along the movement path related to obstacle placement; and the existence of obstacle-distance invariant focal points where mean trajectories intersect in the frontal and vertical planes.

Introduction

When humans move and manipulate objects, their hand paths are smooth, but also highly flexible. Humans do not move in a jerky, robot-like way that is sometimes humorously invoked to illustrated "unnatural" movement behavior. In fact, humans have a hard time making "arbitrary" movements. Even when they scribble freely in three dimensions, their hand moves in a regular way that is typically piecewise planar [1,2]. Movement generation by the nervous systems, the neuro-muscular systems, and the body is constrained by implied laws of motion signatures which are found empirically through invariances of movement trajectories and movement paths. Among these, laws decoupling space and time are of particular importance. For instance, the fact that the trajectories of the hand have approximately bell-shaped velocity profiles across varying movement amplitudes [3] implies a scaling of the time dependence of velocity. The 2/3 power law [4] establishes an analogous scaling of time with the spatial path of the hand's movement. Similarly, the isochrony principle [5] captures that the same spatial segment of a movement takes up the same proportion of movement time as movement amplitude is rescaled. Several of these invariances can be linked to geometrical invariance principles [6].

These invariances imply that movements as a whole have a reproducible temporal form, which can be characterized by movement parameters. Their values are specified before a movement begins, so that one may predict the movement's time course and path based on just an initial portion of the trajectory [7]. Movement parameters are assumed to reside at the level of end-effector trajectories in space and their neural encoding begins to be known [8–10]. The set of possible movements can thus be spanned by a limited number of such parameters. Moreover, the choices of these movement parameters are constrained. For instance, in sequences of movements, earlier segments predict later segments [11].

A key source of variance of kinematic variables is, of course, the time course of the movement itself. The invariance principles suggest that this source of variance can be disentangled from the variation induced when the movement task varies. In this paper, we will first address time as a source of variance, focussing on a fixed movement task, and then use the methods developed to address how movements vary when the task is varied.

Given a fixed movement task, movement trajectories also vary across individuals. Individual differences in movement, a personal movement style, are reproducible and stable over time, as witnessed, for instance, by the possibility to identify individuals or individual characteristics such as gender by movement information alone [12–14].

A third source of variation are fluctuations in how movements are performed from trial to trial or across movement cycles in rhythmic movements. Such fluctuations are of particular interest to movement scientists, because they reflect not only sources of random variability such as neural or muscular noise, but also the extent to which the mechanisms of movement generation stabilize movement against such noise. Instabilities in patterns of coordination have been detected by an increase of fluctuations [15] and differences in variance among different degrees of freedom have been used to establish priorities of neural control [16,17].

A systematic method to disentangle these three sources of movement variation, time, individual differences, and fluctuations, would be a very helpful research tool. Such a method would decompose sets of observed kinematic time series into a common trajectory (that may be specific to the task), participant-specific movement traits, and random

effects. Given the observed decoupling of space and time, such a decomposition would also separate the rescaling of time across these three factors from the variation of the spatial characteristics of movement.

The statistical subfield that deals with analysis of temporal trajectories is the field of functional data analysis. In the literature on functional data, the typical approach for handling continuous signals with time-warping effects is to pre-align samples under an oversimplified noise model in the hope of eliminating the effects of movement timing [18]. In contrast, we propose an analytic framework in which the decomposition of the signal is done simultaneously with the estimation of movement timing effects, so that samples are continually aligned under an estimated noise model. Furthermore, we account for both the task-dependent variation of movement and for individual differences (a brief review of warping in the modeling of biological motion is provided in the Methods section).

Decomposition of time series into a common effect (the time course of the movement given a fixed task), an individual effect, and random variation naturally leads to a mixed-effects formulation [19]. The addition of nonlinear timing effects gives the model the structure of a hierarchical nonlinear mixed-effects model [20]. We present a framework for maximum-likelihood estimation in the model and demonstrate that the method leads to high-quality templates that foster subsequent analysis (e.g., classification). We then show that the results of this analysis can be combined with other models to test hypotheses about the invariance of movement patterns across participants and task conditions. We demonstrate this by using the individual warping functions in a novel factor analysis model that captures variation of movement trajectories with task conditions.

We use as of yet unpublished data from a study of naturalistic movement that extends published work [21]. In the study, human participants transport a wooden cylinder from a starting to a target location while avoiding obstacles at different spatial positions along the path. Earlier work has shown that movement paths and trajectories in this relatively unconstrained, naturalistic movement task clearly reflect typical invariances of movement generation, including the planar nature of movement paths, spatiotemporal invariance of velocity profiles, and a local isochrony principle that reflects the decoupling of space and time [21]. By varying the obstacle configuration, the data include significant and non-trivial task-level variation. We begin by modeling a one-dimensional projection of the time courses of acceleration of the hand in space, which we decompose into a common pattern and the deviations from it that characterize each participant. The timing of the acceleration profiles is determined by individual time warping functions which are of higher quality than conventional estimates, since timing and movement noise are modeled simultaneously. The high quality of the estimates is demonstrated by classifying movements according to participant. Finally, the results of the nonlinear mixed model are analyzed using a novel factor analysis model that estimates a low-dimensional subspace within which movement paths change when the task conditions are varied. This combination of statistical models makes it possible to separate and visualize the variation caused by experimental conditions, participants and repetition. Furthermore, we can formulate and test hypotheses about the effects of experimental conditions on movement paths. Using the proposed statistical models, we document three findings: a linearly amplified deviation in mean path related to increase in obstacle height; a consistent asymmetric pattern of variation along the movement path related to obstacle placement; and the existence of obstacle-distance invariant focal points where mean trajectories intersect in the frontal and vertical plane.

Software for performing the described types of simultaneous analyses of timing and movement effects are publicly available through the `pavpop` R package [22]. A short guide on model building and fitting in the proposed framework is available in Supporting Information, along with an application to handwritten signature data.

Methods

Experimental data set

Ten participants performed a series of simple, naturalistic motor acts in which they moved a wooden cylinder from a starting to a target position while avoiding a cylindric obstacle. The obstacle's height and positition along the movement path were varied across experiments (Figure 1.)

The movements were recorded with the Visualeyez (Phoenix Technologies Inc.) motion capture system VZ 4000. Two trackers, each equipped with three cameras, were mounted on the wall 1.5 m above the working surface, so that both systems had an excellent view of the table. A wireless infrared light-emitting diode (IRED) was attached to the wooden cylinder. The trajectories of markers were recorded in three Cartesian dimensions at a sampling rate of 110 Hz based on a reference frame anchored on the table. The starting position projected to the table was taken as the origin of each trajectory in three-dimensional Cartesian space. Recorded movement paths for two experimental conditions are shown in Figure 2. The acceleration profiles considered in the following sections were obtained by using finite difference approximations of the raw velocity magnitude data, see Figure 3.

Obstacle avoidance was performed in 15 different conditions that combined three obstacle heights S, M, or T with five distances of the obstacle from the starting position $d \in \{15, 22.5, 30, 37.5, 45\}$. A control condition had no obstacle. The participants performed each condition 10 times. Each *experimental condition* provided $n = 100$ functional samples for a total of $n_f = 1600$ functional samples in the dataset, leading to a total data size of $m = 175,535$ observed time points.

The present data set is described in detail in [23]. The experiment is a refined version of the experiment described in [21].

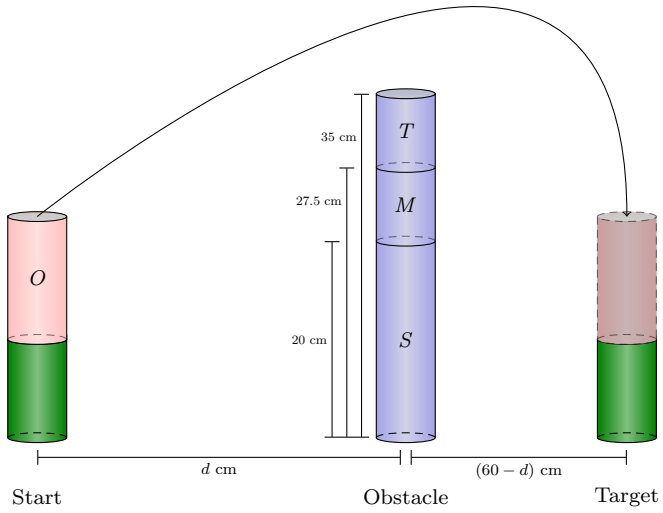

Figure 1. Obstacle avoidance paradigm. Participants move the cylindrical object O from the starting platform (green) to the target platform by lifting it over an obstacle. Obstacles of three different heights, small (S), medium (M), and tall (T), were used in the experiment, and the distance from starting position to obstacle d was varied.

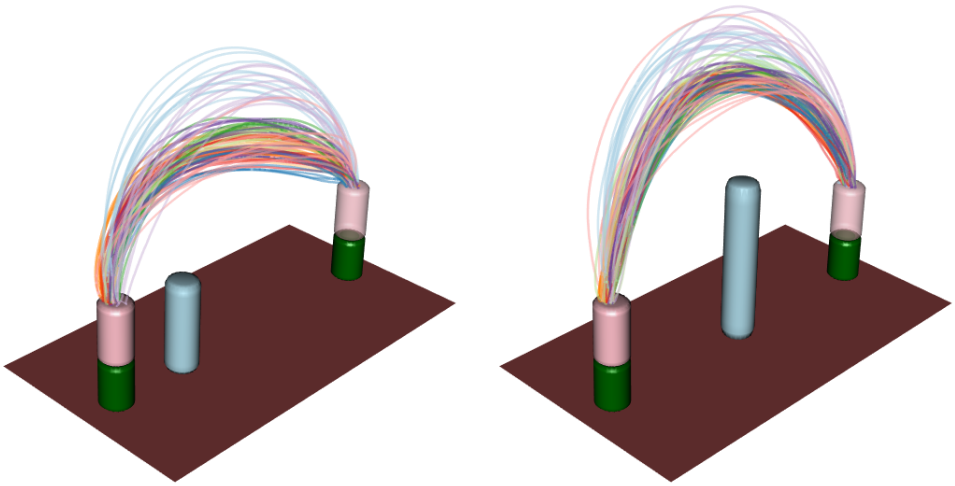

(a) Experiment $d = 15,\ S$ **(b)** Experiment $d = 30,\ T$

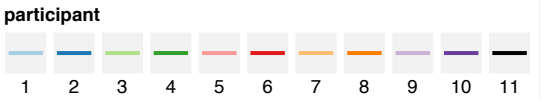

Figure 2. Recorded paths of the hand-held object in space for two experimental conditions.

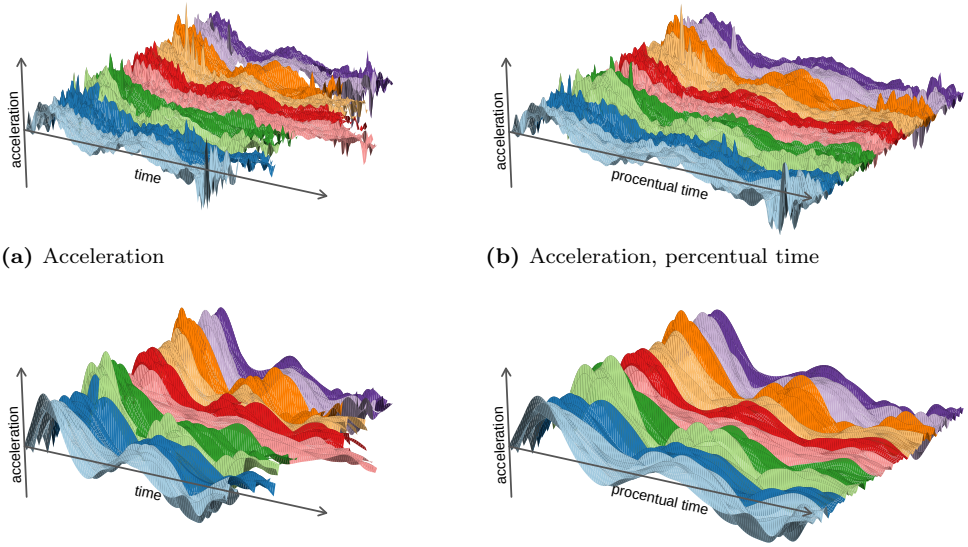

(a) Acceleration **(b)** Acceleration, percentual time

(c) Smoothed acceleration **(d)** Smoothed acceleration, percentual time

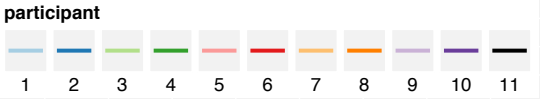

Figure 3. Surface plots of acceleration profiles ordered by repetition (y-axis) in the experiment with $d = 30,\ T$. The plots allow visualization of the variation across participants and repetitions.

Time warping of functional data

Not every movement has the exact same duration. Comparisons across movement conditions, participants, and repetitions are hampered by the resulting lack of alignment of

the movement trajectories. For a single condition, this is illustrated in Figure 3 (a) and (c), in which the duration of the movement clearly varies from participant to participant but also from repetition to repetition. Without alignment, it is difficult to compare movements. In an experiment such as the present, in which start and target positions are fixed, the standard solution for aligning samples is to use *percentual time*; the onset of the individual movement corresponds to time 0% and the end of the movement to time 100%. Such linear warping is based on detecting movement onset and offset through threshold criteria. As can be seen in Figure 3 (b) and (c), linear warping does not align the characteristic features of the acceleration signals very well, however, as there is still considerable variation in the times at which acceleration peaks. There is, in other words, a nonlinear component to the variation of timing.

To handle nonlinear variation of timing, the signal must be time warped based on an estimated, continuous, and monotonically increasing function that maps percentual time to warped percentual time, such that the functional profiles of the signals are best aligned with each other. Such warping has traditionally been achieved by using the dynamic-time warping (DTW) algorithm [24] which offers a fast approach for globally optimal alignment under a prespecified distance measure(for reviews of time warping in the domains of biological movement modeling see [25, 26]). DTW is both simple and elegant, but while it will often produce much better results than cross-sectional comparison of time-warped curves [27–29], it does suffer from some problems. In particular, DTW requires a pointwise distance measure such as Euclidean distance. Therefore, the algorithm cannot take serially correlated noise effects in a signal into account. As a result, basic unconstrained DTW will overfit in the sense of producing perfect fits whenever possible, and for areas that cannot be perfectly matched, either stretch them or compress them to a single point. In other words, DTW cannot model curves with systematic amplitude differences, and using DTW to naively computing time warped mean curves is in general problematic [30, 31]. This lacking ability to model serial correlated effects can be somewhat mitigated by restricting the DTW step pattern, in particular through a reduced search window for the warping function and constraints on the maximal step sizes. These are, however, hard model choices, they are restrictions on the set of possible warping functions, and they are a difficult to interpret since they seek to fix a problem in amplitude variation by penalizing warping variation. Instead, a much more natural approach would be to use a data term that models the amplitude variation encountered in data, and to impose warp regularization by using a cost function that puts high cost on undesired warping functions. In the following sections, we will propose a model with these properties, which, in addition, allows for estimating the data term, warp regularization and their relative weights from the data.

To illustrate the difference between DTW and the proposed method, consider the example displayed in Figure 4 where the recorded z-coordinates (elevation) of one participant's 10 movements in the control condition (without obstacle) are plotted in recorded time (a) and percentual time (b). These samples have been aligned using DTW by iteratively estimating a pointwise mean function and aligning the samples to the mean function (10 iterations). The three rows of Figure 5 display the results of the procedure using three different step patterns. We first note the strong overfitting of the symmetric and asymmetric step patterns, where the sequences with highest elevation are collapsed to minimize the residual. Secondly, we note the jagged warping functions that are results of the discrete nature of the DTW procedure. For comparison, we fitted a variant of the proposed model with a continuous model for the warping function controlled by 13 basis functions. We modeled both amplitude and warping effects as random Gaussian processes using simple, but versatile classes of covariance functions (see Supporting Information), and estimated the internal weighting of the effect directly from the samples. The results are displayed in Figure 6. We see that the warped elevation trajectories seem perfectly aligned, and that the corresponding warping functions are relatively simple, with the majority of variation being near the end of the movement. It is evident from the figures that both the alignment is much more reasonable, and the warping functions are much simpler than the warping functions found using DTW.

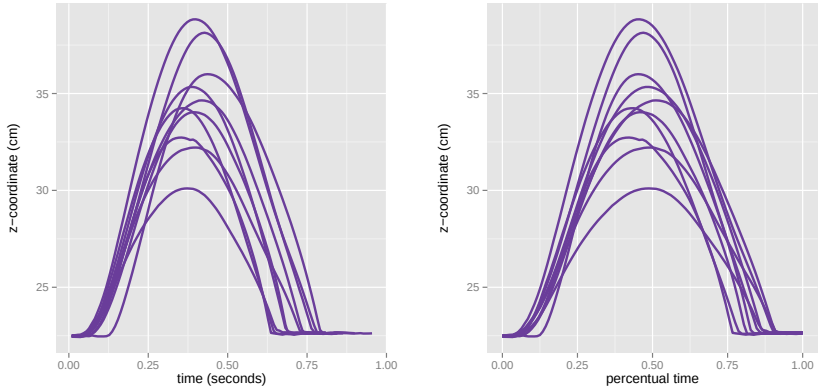

(a) Recorded z-coordinate, observed time **(b)** Recorded z-coordinate, percentual time

Figure 4. Elevation (z-dimension) for one participant's (no.10) repetitions of the control condition without obstacle plotted on different time scales.

Two questions naturally arise. Firstly, are the warping functions unique? Other warping functions could perhaps have produced similarly well-aligned data. Secondly, do we want perfectly aligned trajectories? There is still considerable variation of the amplitude in the warped z-coordinates of the movement trajectories in Figure 4 (c), for instance. Some of the variation visible in the unwarped variant in Figure 4 (b) could be due to random variations in amplitude rather than timing.

Using the time-warping functions that were determined by aligning the z-coordinates of the movements to now warp the trajectories for the x- and y-coordinates (Figure 7), we see that the alignment obtained is not perfect. Conversely, were we to use warping functions determined for the x- or y-coordinate to warp the z-coordinate we would encounter similarly imperfect alignment. Thus, we need a method that avoids over-aligning, and represents a trade-off between the complexity of the warping functions and of the amplitude variation in data. In the next section, we introduce a statistical model that handle this trade-off in a data-driven fashion by using the patterns of variation in the data to find the most likely separation of amplitude and timing variation.

Statistical modeling of movement data to achieve time warping

In the following, we describe inference for a single experimental condition. For a given experimental condition—an object that needs to be moved to a target and an obstacle that needs to be avoided—we assume there is a common underlying pattern in all acceleration profiles; all $n_p = 10$ participants will lift the object and move it toward the target, lifting it over the obstacle at some point. This assumption is supported by the pattern in the data that Figure 3 visualizes. We denote the hypothesized underlying acceleration profile shared across participants and repetitions by θ. In addition to this fixed acceleration profile, we assume that each participant, i, has a typical deviation φ_i from θ, so that the acceleration profile that is characteristic of that participant is $\theta + \varphi_i$. Such a systematic pattern characteristic of each participant is apparent in Figure 3 (c) and (d). The individual trials (repetitions) of the movement deviate from this characteristic profile of the individual. We model these deviations as additive random effects with serial correlations so that for each repetition, j, of the experimental condition we have an additive random effect x_{ij} that causes deviation from the ideal profile. Finally we assume that the data contains observation noise ε_{ij} tied to the tracking system and data processing.

Time was implicit, up to this point, and the observed acceleration profile was decomposed into additive, linear contributions. We now assume, in addition, that each participant, i, has a consistent timing of the movement across repetitions, that is reflected in the temporal deformation of the acceleration profile (Figure 3 (a) and (c)) and is captured by the time warping function ν_i. On each repetition, j, of the condition, the

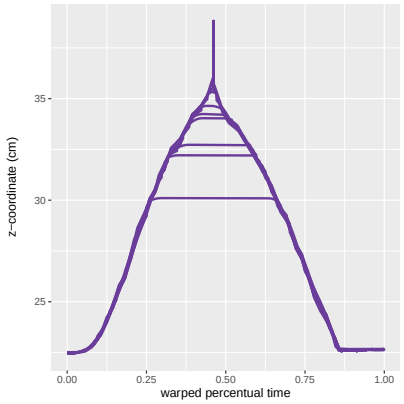

(a) Recorded z-coordinate, warped percentual time, DTW symmetric step pattern

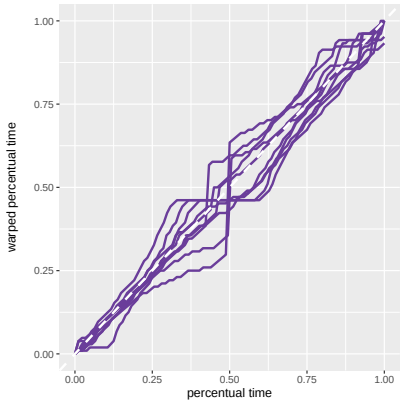

(b) Warping functions, white dashed line shows the identity, DTW symmetric step pattern

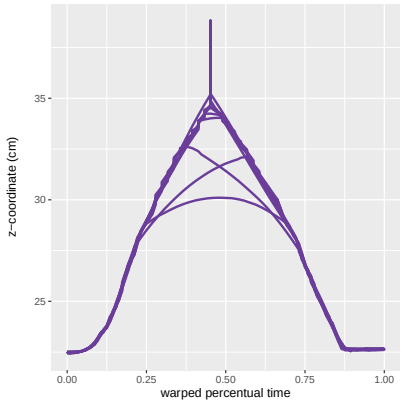

(c) Recorded z-coordinate, warped percentual time, DTW asymmetric step pattern

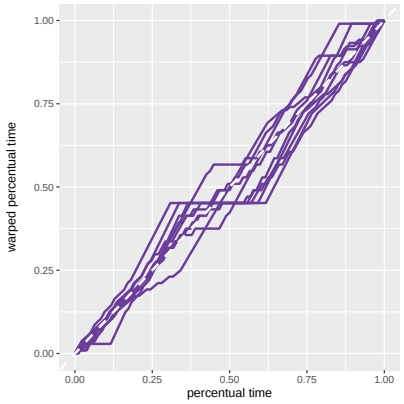

(d) Warping functions, white dashed line shows the identity, DTW asymmetric step pattern

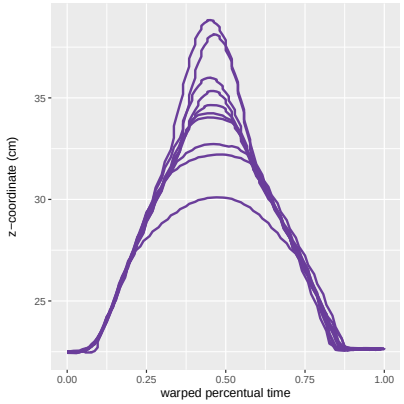

(e) Recorded z-coordinate, warped percentual time, DTW Sakoe-Chiba step pattern

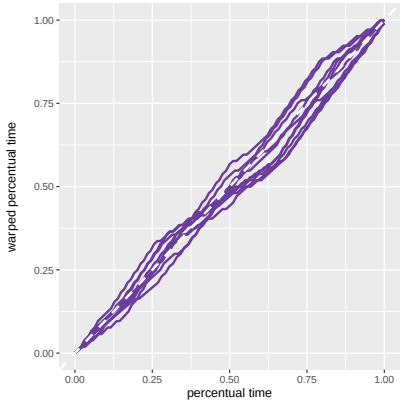

(f) Warping functions, white dashed line shows the identity, DTW Sakoe-Chiba step pattern

Figure 5. The elevation trajectories from Figure 4 warped with dynamic time warping using different step patterns. *Symmetric* step pattern denotes the so-called White-Neely step pattern that has no local constraints, *asymmetric* step pattern denotes a slope-constrained step pattern where local slopes are required to be between 0 and 2, and *Sakoe-Chiba* step pattern denotes the asymmetric step pattern proposed in [24, Table I] with a slope constraint of 2.

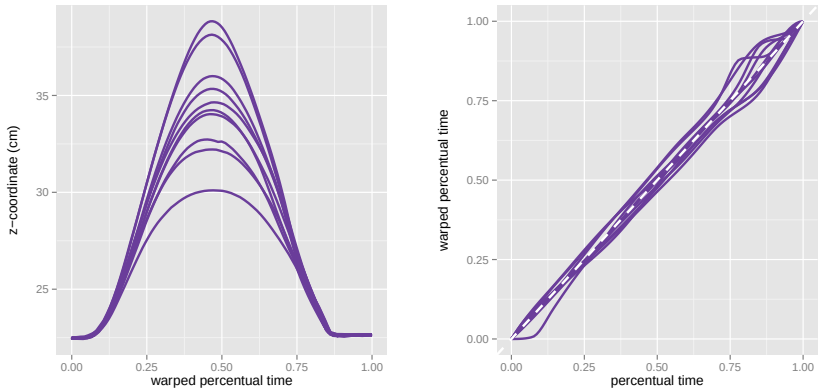

(a) Recorded z-coordinate, warped percentual time, proposed model

(b) Warping functions, white dashed line shows the identity, proposed model

Figure 6. The elevation trajectories from Figure 4 warped with the proprosed model.

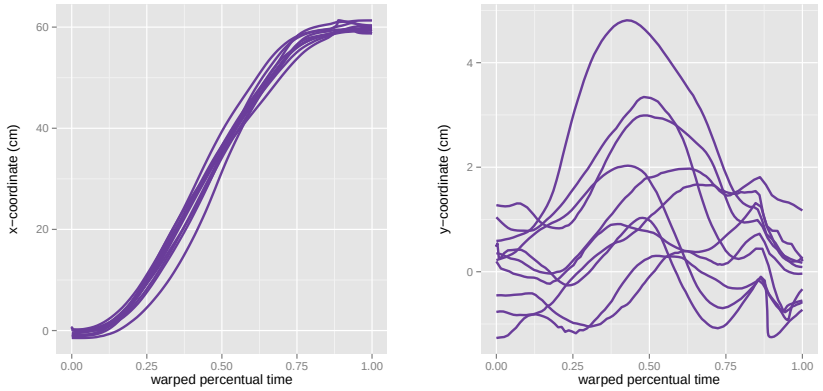

(a) Recorded x-coordinate, warped percentual time

(b) Recorded y-coordinate, warped percentual time

Figure 7. The other two spatial coordinates, x, and y, of the movements from Figure 4 (a) warped with the warping functions from Figure 6, that was estimated from the elevation component z.

timing of participant, i, contains a random variation of timing around ν_i captured by a random warping function v_{ij} (see Figure 3).

Altogether, we have described the following statistical model of the observed acceleration profiles across participants:

$$y_{ij}(t) = (\theta + \varphi_i) \circ (\nu_i + v_{ij})(t) + x_{ij}(t) + \varepsilon_{ij}(t) \tag{1}$$

where $\circ$ denotes functional composition, t denotes time, θ, φ_i, $\nu_i : \mathbb{R} \to \mathbb{R}$ are fixed effects and v_{ij}, x_{ij} and ε_{ij} are random effects. The serially correlated effect x_{ij} is assumed to be a zero-mean Gaussian process with a parametric covariance function $\mathcal{S} : \mathbb{R} \times \mathbb{R} \to \mathbb{R}$; the randomness of the warping function v_{ij} is assumed to be completely characterized by a latent vector of n_w zero-mean Gaussian random variables $\boldsymbol{w}_{ij}$ with covariance matrix $\sigma^2 C$; and ε_{ij} is Gaussian white noise with variance σ^2.

Compared to conventional methods for achieving time warping, the proposed model (1) models amplitude and warping variation between repetition as random effects, which enables separation of the effects from the joint likelihood. Conventional approaches for warping model warping functions as fixed effects and do not contain amplitude effects [18]. The idea of modeling warping functions as random effects have previously been considered by [32–34] where warps were modeled as random shifts or random polynomials. None of these works however included amplitude variation. Recently, some works have considered models with random affine transformations for warps and amplitude variation in relation to growth curve analysis [35,36]. A generalization that does not require affine transformations for warp and amplitude variation is presented in [37]. The presented model (1) is a hierarchical generalization of the model presented in [37]. In the context of aligning image sequences in human movement analysis, morphable models [29,38] model an observed movement pattern as a linear combination of prototypical patterns using both nonlinear warping functions (estimated using DTW) and spatial shifts. Thus morphable models are similar to the warping approaches that model both warp and amplitude effects as fixed [39].

Maximum likelihood estimation of parameters

Model (1) has a considerable number of parameters, both for linear and nonlinear dependencies on the underlying state variable acceleration. The model also has effects that interact. This renders direct simultaneous likelihood estimation intractable. Instead we propose a scheme in which fixed effects and parameters are estimated and random effects are predicted iteratively on three different levels of modeling.

Nonlinear model At the nonlinear level, we consider the original model (1), and simultaneously perform conditional likelihood estimation of the participant-specific warping functions and predict the random warping functions from the negative log posterior. All other parameters remain fixed.

Fixed warp model At the fixed warp level, we fix the participant-specific warping effect ν_i at the conditional maximum likelihood estimate, and the random warping function v_{ij}, at the predicted values. The resulting model is an approximate linear mixed-effects model with Gaussian random effects x_{ij} and ε_{ij}, that allows direct maximum-likelihood estimation of the remaining fixed effects, θ and φ_i.

Linearized model At the linearized level, we consider the first-order Taylor approximation of model (1) in the random warp v_{ij}. This linearization is done around the estimate of ν_i plus the given prediction of v_{ij} from the nonlinear model. The result is again a linear mixed-effects model, for which one can compute the likelihood explicitly, while taking the uncertainty of all random effects—including the nonlinear effect v_{ij}—into account. At this level all variance parameters are estimated using maximum-likelihood estimation.

The estimation/prediction procedure is inspired by the algorithmic framework proposed in [37]. The estimation procedure is, however, adapted to the hierarchical structure of data and refined in several respects. On the linearized model level, the nonlinear Gaussian random effects are approximated by linear combinations of correlated Gaussian variables

around the mode of the nonlinear density. The linearization step thus corresponds to a Laplace approximation of the likelihood, and the quality of this approximation is approximately second order [40].

Let $\boldsymbol{y}_{ij}$ be the vector of the m_{ij} observations for participant i's jth replication of the given experimental condition, and let $\boldsymbol{y}_i$ denote the concatenation of all functional observations of participant i in the experimental condition, and $\boldsymbol{y}$ the concatenation all these observations across participants. We denote the lengths of these vectors by m_i and m. Furthermore, let $\sigma^2 S_{ij}$, $\sigma^2 S_i$ and $\sigma^2 S$ denote the covariance matrices of $\boldsymbol{x}_{ij} = (x_{ij}(t_k))_k$, $\boldsymbol{x}_i = (\boldsymbol{x}_{ij})_j$, and $\boldsymbol{x} = (\boldsymbol{x}_i)_i$ respectively. We note that the index set for k depends on i and j since the covariance matrices S_{ij} vary in size due to the different durations of the movements and because of possible missing values when markers are occluded.

We note that all random effects are scaled by the noise standard deviation σ. This parametrization is chosen because it simplifies the likelihood computations, as we shall see. Finally, we denote the norm induced by a full-rank covariance matrix A by $\|\boldsymbol{z}\|_A^2 = \boldsymbol{z}^\top A^{-1}\boldsymbol{z}$.

Fixed warp level We model the underlying profile, θ, and the participant-specific variation around this trajectory, φ_i, in the common (warped) functional basis $\boldsymbol{\Phi} \in \mathbb{R}^{m\times K}$, with weights $\boldsymbol{c} = (c_1, \ldots, c_K)$ for θ and $\boldsymbol{d}_i = (d_{i1}, \ldots, d_{iK})$ for φ_i. We assume that the participant-specific variations, φ_i, are centered around θ and thus $\sum_i \boldsymbol{d}_i = \boldsymbol{0} \in \mathbb{R}^K$. Furthermore, the square magnitude of the weights, $\boldsymbol{d}_i$, is penalized with a weighting factor η. This penalization helps guiding the alignment process in the direction of the highest possible level of detail in the common profile θ when the initial alignment is poor.

For fixed warping functions ν_i and v_{ij}, the negative log likelihood function in $\theta = \boldsymbol{\Phi c}$ is proportional to

$$\ell(\boldsymbol{c}) = \|\boldsymbol{y} - \boldsymbol{\Phi c}\|^2_{\mathbb{I}_n + S}$$

where $\mathbb{I}_n$ denotes the $n \times n$ identity matrix. This yields the estimate

$$\hat{\boldsymbol{c}} = (\boldsymbol{\Phi}^\top(\mathbb{I}_m + S)^{-1}\boldsymbol{\Phi})^{-1}\boldsymbol{\Phi}^\top(\mathbb{I}_m + S)^{-1}\boldsymbol{y}.$$

The penalized negative profile log likelihood for the weights $\boldsymbol{d}_i$ for φ_i is proportional to

$$\ell(\boldsymbol{d}_i) = \|\boldsymbol{y}_i - \boldsymbol{\Phi}_i(\hat{\boldsymbol{c}} + \boldsymbol{d}_i)\|^2_{I_{m_i}+S_i} + \eta \boldsymbol{d}_i^\top \boldsymbol{d}_i,$$

which gives the maximum likelihood estimator

$$\hat{\boldsymbol{d}}_i = (\boldsymbol{\Phi}_i^\top(\mathbb{I}_{m_i} + S_i)^{-1}\boldsymbol{\Phi}_i + \eta\mathbb{I}_K)^{-1}\boldsymbol{\Phi}_i^\top(\mathbb{I}_{m_i} + S_i)^{-1}(\boldsymbol{y}_i - \boldsymbol{\Phi}_i\hat{\boldsymbol{c}}).$$

Nonlinear level Similarly to the linear mixed-effects setting [41], it is natural to predict nonlinear random effects from the posterior [20], since these predictions correspond to the most likely values of the random effects given the observed data. Recall that the Gaussian variables, $\boldsymbol{w}_{ij}$, parametrize the randomness of the repetition-specific warping function v_{ij}. Since the conditional negative (profile) log likelihood function in ν_i given the random warping function v_{ij} and the negative (profile) log posterior for $\boldsymbol{w}_{ij}$ coincide, we propose to simultaneously estimate the fixed warping effects ν_i and predict the random warping effects v_{ij} from the joint conditional negative log likelihood/negative log posterior which is proportional to

$$p(\nu_i, \boldsymbol{w}_{ij}) = \sum_j \|\boldsymbol{y}_{ij} - (\hat{\theta} + \hat{\varphi}_i) \circ (\nu_i + v_{ij})(t_k)_k\|^2_{\mathbb{I}_{n_{ij}}+S_{ij}} + \sum_j \|\boldsymbol{w}_{ij}\|^2_C. \tag{2}$$

Since the variables $\boldsymbol{w}_{ij}$ can be arbitrarily transformed through the choice of warping function v_{ij}, the assumption that variables are Gaussian is merely one of computational convenience.

Linearized level We can write the local linearization of model (1) in the random warping parameters $\boldsymbol{w}_{ij}$ around a given prediction $\boldsymbol{w}_{ij}^0$ as a vectorized linear mixed-effects model

$$\boldsymbol{y} \approx \boldsymbol{\vartheta} + Z(\boldsymbol{w} - \boldsymbol{w}^0) + \boldsymbol{x} + \boldsymbol{\varepsilon} \tag{3}$$

with effects given by

$$\boldsymbol{\vartheta} = \{(\theta + \varphi_i) \circ (\nu_i + v_{ij}^0)(t_k)\}_{ijk} \in \mathbb{R}^m,$$

$$Z = \operatorname{diag}(Z_{ij})_{ij}, \qquad Z_{ij} = \{\partial_{\boldsymbol{t}}(\theta + \varphi_i) \circ (\nu_i + v_{ij}^0)(t_k)(\nabla_{\boldsymbol{w}} v_{ij}^0(t_k))^\top\}_k \in \mathbb{R}^{m_i \times n_w},$$

$$\boldsymbol{w} = (\boldsymbol{w}_{ij})_{ij} \sim \mathcal{N}_{n_p n_{\boldsymbol{w}}}(0, \sigma^2 \mathbb{I}_{n_p} \otimes C), \qquad \boldsymbol{x} \sim \mathcal{N}_m(0, \sigma^2 S), \qquad \boldsymbol{\varepsilon} \sim \mathcal{N}_m(0, \sigma^2 \mathbb{I}_m),$$

where v_{ij}^0 indicates that the warping function is evaluated at the prediction $\boldsymbol{w}_{ij}^0$, $\operatorname{diag}(Z_{ij})_{ij}$ is the block diagonal matrix with the Z_{ij} matrices along its diagonal, and $\otimes$ denotes the Kronecker product.

Altogether, twice the negative profile log likelihood function for the linearized model (3) is

$$\ell(\sigma^2, C, S) = m \log \sigma^2 + \log\det V + \sigma^{-2} \|\boldsymbol{y} - \hat{\boldsymbol{\vartheta}} + Z\boldsymbol{w}^0\|_V^2 \tag{4}$$

where $V = S + Z(\mathbb{I}_n \otimes C)Z^\top + \mathbb{I}_m$.

Modeling of effects and algorithmic approach

So far, the model (1) has only been presented in a general sense. We now consider the specific modeling choices. The acceleration data has been rescaled using a common scaling for all experimental conditions, such that the span of data values has length 1 and the global timespan is the interval $[0, 1]$.

To model the amplitude effects, we use a cubic B-spline basis $\boldsymbol{\Phi}$ with K knots [42].

We require that the fixed warping function ν_i is an increasing piecewise linear homeomorphism parametrized by n_w equidistant anchor points in $(0, 1)$, and assume that v_{ij} is of the form

$$v_{ij}(t) = t + \mathcal{E}_{ij}(t),$$

where $\mathcal{E}_{ij}(t)$ is the linear interpolation at t of the values $\boldsymbol{w}_{ij}$ placed at the n_w anchor points in $(0, 1)$. In the given experimental setting, the movement path is fixed at the onset and the end of the movement. The movement starts when the cylindrical object is lifted and ends when it is placed at its target position. Thus, we would expect the biggest variation in timing to be in the middle of the movement (in percentual time). These properties can be modeled by assuming that $\boldsymbol{w}_{ij}$ is a discretely observed zero-drift Brownian bridge with scale $\sigma^2\gamma^2$ [43, Chapters 8-9], which means that the covariance matrix $\sigma^2 C$ is given by point evaluation of the covariance function

$$\mathcal{C}(t, t') = \sigma^2\gamma^2\, t(1 - t')$$

for $t \leq t'$. When predicting the warps from the negative log posterior we restrict the search space to warps ν_i and $\nu_i + v_{ij}$ that are increasing homeomorphic maps of the domain $[0, 1]$ onto itself. The conditional distribution of ν_{ij} given this restriction is slightly changed. For the used numbers of anchor points n_w and the estimated variance parameters the difference is however minuscule, and we use the original Brownian model as a high-quality approximation of the true distribution.

We assume that the sample paths of the serially correlated effects x_{ij} are continuous and that the process is stationary [44]. A natural choice of covariance is then the Matérn covariance with smoothness parameter μ, scale $\sigma^2\tau^2$ and range $1/\alpha$ [45], since it offers a broad class of stationarity covariance functions.

Finally, in order to consistently penalize the participant-specific spline across experimental conditions with varying variance parameters, we will use penalization weights that are normalized with the variance of the amplitude effects, $\eta = \lambda/(1 + \tau^2)$.

Algorithm 1 Maximum likelihood estimation for model (1)

procedure MLE($\boldsymbol{y}$, η, τ^2, α, γ^2)
  Compute $\hat{\theta}$ and $\hat{\varphi}_1, \ldots, \hat{\varphi}_m$ assuming an identity warp ▷ Initialize
  for $i = 1, \ldots, i_{\max}$ **do** ▷ Outer iterations
    for $j = 1, \ldots, j_{\max}$ **do** ▷ Inner iterations
      Estimate and predict warping functions by minimizing the posterior (2)
      if Estimates and predictions do not change **then break**
      end if
      Recompute $\hat{\theta}$ and $\hat{\varphi}_1, \ldots, \hat{\varphi}_m$
    end for
    Estimate variance parameters by minimizing the linearized likelihood (4)
  end for
  return $\hat{\theta}$, $\hat{\varphi}_1, \ldots, \hat{\varphi}_m$, $\hat{\nu}_1, \ldots, \hat{\nu}_m$, $\hat{\sigma}^2$, $\hat{\eta}$, $\hat{\tau}^2$, $\hat{\alpha}$, $\hat{\gamma}^2$ ▷ Maximum likelihood estimates
end procedure

The algorithm for doing inference in model (1) is outlined in Algorithm 1. We have found that $i_{\max} = j_{\max} = 5$ outer and inner loops are sufficient for convergence. A wide variety of these types of models can be fitted using the `pavpop` R package [22]. A short guide on model building and fitting is available in Supporting Information.

In the following we consider two approaches, with (1) samples parametrized by recorded time (Figure 3a) and (2) samples parametrized by percentual time (Figure 3b). Parameters for the latter case will be denoted by a subscript p.

The number of basis functions K, the number of warping anchor points n_w, and the regularization parameter λ were determined by the average 5-fold cross-validation score on each of three experimental conditions ($d = 30$ cm and obstacle heights S, M, and T). The models were fitted using the method described in the previous section, and the quality of the models was evaluated through the accuracy of classifying the participant from a given movement in the test set, using posterior distance between the sample and the combined estimates for the fixed effects $(\theta + \varphi_i) \circ \nu_i$. The cross-validation was done over a grid of the following values $\mu, \mu_{\mathrm{p}} \in \{0.5, 1, 2\}$, $K \in \{8, 13, 18, 23, 28, 33\}$, $K_{\mathrm{p}} \in \{8, 9, \ldots, 18\}$, $n_w, n_{w\mathrm{p}} \in \{0, 1, 2, 3, 5, 10\}$, $\lambda, \lambda_{\mathrm{p}} \in \{0, 1, 2, 3\}$. The best values were found to be $\mu = 2$, $K = 23$, $n_w = 2$, $\lambda = 2$ and $\mu_{\mathrm{p}} = 1$ $K_{\mathrm{p}} = 12$, $n_{w\mathrm{p}} = 1$, $\lambda_{\mathrm{p}} = 0$. We note that the smoothness parameter $\mu = 2$ is on the boundary of the cross-validation grid. The qualitative difference between second order smoothness $\mu = 2$ (corresponding to twice differentiable sample paths of amplitude effects) and higher order is so small, however, that we chose to ignore higher order smoothness. Furthermore, $\lambda_{\mathrm{p}} = 0$ indicates that we do not need to penalize participant-specific amplitude effects when working with percentual time. The reason is most likely that the samples have better initial alignment in percentual time. The estimated participant-specific acceleration profiles using percentual time can be seen in Figure 8.

A simulation study that validates the method and implementation on data simulated using the maximum likelihood estimates of the central experimental condition ($d = 30.0$ cm, medium obstacle) is available in Supporting Information.

Results

Identification of individual differences

A first assessment of the strength of the statistical model (1) is to examine the extent to which the model captures individual differences. Proper modeling of systematic individual differences is not only of scientific interest per se, but also provides perspective for interpreting any observed experimental effects. To validate the capability of the model to capture systematic individual differences, we use the model to identify an individual from the estimated individual templates. Such identification of individuals is becoming increasingly relevant also in a practical sense with the recent technological advances in motion tracking systems, and the growing array of digital sensors in handheld consumer

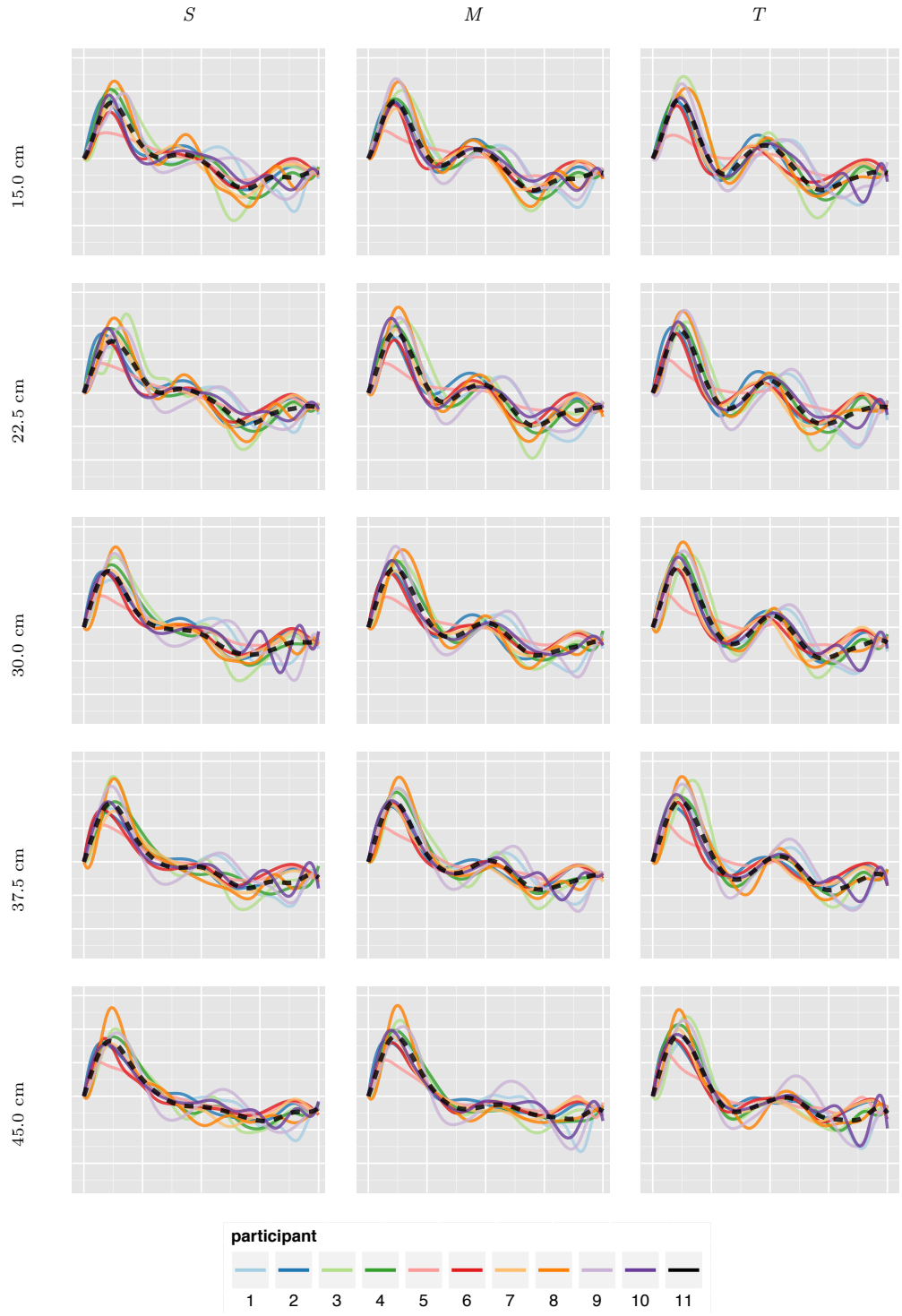

Figure 8. Estimated fixed effects $(\theta + \varphi_i) \circ \nu_i$ in the 15 obstacle avoidance experiments using percentual time. The dashed trajectory shows the estimate for θ. The average percentual warped time between two white vertical bars corresponds to 0.2 seconds.

electronics. Consistent with the framing of model (1), we perform identification of individual participants on the basis of the data from a single experimental condition. This is, in a sense, a conservative approach. Combining data across the different conditions of the experimental tasks would likely provide more discriminative power given that personal movement styles tend to be reproducible.

The classification of the movement data is based on the characteristic acceleration profile computed for each participant. For this to work it is important that individual movement differences are not smoothed away. The hyperparameters of the model were chosen with this requirement in mind. In the following, we describe alternative methods we considered. For all approaches, the stated parameters have been chosen by 5-fold cross-validation on the experimental conditions with obstacle distance $d = 30.0$ cm. The grids used for cross-validation are given in Supporting Information section. Recall that subscript p indicates the use of percentuall time.

Nearest Participant (NP) NP classification classifies using the minimum combined pointwise L^2 distance to all samples for every individual in the training set.

Modified Band Median (MBM) MBM classification estimates templates using the modified band median proposed in [46], which under mild conditions is a consistent estimator of the underlying fixed amplitude effects warped according to the modified band medians of the warping functions. Classification is done using L^2 distance to the estimated templates. In the computations we count the number of bands defined by $J = 4$ curves [46, Section 2.2]. MBM_p used $J_\text{p} = 2$.

Robust Manifold Embedding (RME) RME classification estimates templates using the robust manifold embedding algorithm proposed in [47], which, assuming that data lies on a low-dimensional smooth manifold, approximates the geodesic distance and computes the empirical Fréchet median function. Classification is done using L^2 distance to the estimated templates.

Dynamic Time Warping (DTW) DTW classification estimates templates by iteratively time warping samples to the current estimated personal template (5 iterations per template) using an asymmetric step pattern (slopes between 0 and 2). The template is modeled by a B-spline with 33 degrees of freedom. DTW_p used 16 degrees of freedom.

Fisher-Rao (FR) FR classification estimates templates as Karcher means under the Fisher-Rao Riemannian metric [48] of the data represented using a single principal component [49]. Čencov's theorem states that the Fisher-Rao distance is the only distance that is preserved under warping [50], and in practice the distance is computed by using a dynamic time warping algorithm on the square-root slope functions of the data. Classification is done using L^2 distance to the estimated templates.

Elastic Fisher-Rao (FR_E) FR_E classification estimates templates analogously to FR, but classifies using the weighted sum of elastic amplitude and phase distances [51, Definition 1 and Section 3.1]. The phase distance was weighted by a factor 1.5. FR_Ep uses two principal components and a phase distance weight of 1.

Timing and Motion Separation (TMS) The proposed TMS classification estimates templates of the fixed effects $(\theta + \varphi_i) \circ \nu_i$ using Algorithm 1. Classification is done using least distance measured in the negative log posterior (2) as a function of the test samples. The parameters were set as described in the previous section.

We evaluate classification accuracy using 5-fold cross-validation, which means that eight samples are available in the training set for every participant. The folds of the cross-validation are chosen chronologically, such that the first fold contains replications 1 and 2, the second contains 3 and 4 and so on. The results are available in Table 1. We see that TMS and TMS_p achieve the highest classification rates, followed by FR_Ep, FR_p and RME_p. Thus, the model enables identification of individual movement style. Furthermore, we note that there is little effect of using percentual time for the proposed method, which for all other methods gives a considerable boost in accuracy. This suggest that the TMS methods align data well without the initial linear warping and the endpoint constraints of percentual time.

d	obstacle	NP	NP_p	MBM	MBM_p	RME	RME_p	DTW	DTW_p	FR	FR_p	FR_E	FR_{Ep}	TMS	TMS_p
15.0 cm	S	0.36	0.48	0.53	0.43	0.55	0.57	0.52	0.52	0.47	0.54	0.62	0.51	0.70	**0.76**
	M	0.36	0.46	0.38	0.45	0.41	0.43	0.49	0.56	0.36	0.49	0.47	0.46	**0.69**	0.66
	T	0.41	0.47	0.41	0.46	0.49	0.50	0.43	0.43	0.32	0.56	0.49	0.49	**0.64**	0.62
22.5 cm	S	0.36	0.49	0.34	0.46	0.37	0.50	0.45	0.44	0.44	0.51	0.50	0.51	**0.70**	0.68
	M	0.38	0.44	0.42	0.53	0.46	0.55	0.38	0.42	0.32	0.45	0.42	0.55	0.62	**0.74**
	T	0.36	0.49	0.45	0.54	0.46	0.57	0.40	0.53	0.48	0.57	0.53	**0.64**	0.61	**0.64**
30.0 cm	S	0.27	0.29	*0.37*	*0.47*	0.41	0.45	*0.43*	*0.44*	*0.40*	*0.43*	*0.46*	*0.55*	*0.63*	***0.65***
	M	0.30	0.42	*0.38*	*0.46*	0.40	0.45	*0.34*	*0.49*	*0.36*	*0.48*	*0.46*	*0.47*	***0.65***	***0.65***
	T	0.37	0.44	*0.42*	*0.50*	0.50	0.45	*0.44*	*0.44*	*0.37*	*0.50*	*0.39*	*0.43*	***0.74***	*0.69*
37.5 cm	S	0.28	0.45	0.41	0.49	0.42	0.51	0.45	0.50	0.36	0.51	0.39	0.56	0.69	**0.74**
	M	0.26	0.33	0.33	0.37	0.35	0.41	0.40	0.49	0.35	0.37	0.32	0.53	0.57	**0.62**
	T	0.31	0.43	0.38	0.43	0.40	0.46	0.37	0.29	0.50	0.48	0.49	0.55	0.63	**0.65**
45.0 cm	S	0.25	0.38	0.33	0.45	0.32	0.42	0.34	0.51	0.32	0.45	0.37	0.41	**0.68**	0.65
	M	0.29	0.31	0.29	0.38	0.38	0.39	0.43	0.43	0.36	0.48	0.38	0.45	0.53	**0.57**
	T	0.29	0.39	0.45	0.48	0.48	0.57	0.38	0.45	0.39	0.44	0.44	0.47	**0.66**	0.58
average		0.323	0.418	0.393	0.460	0.427	0.482	0.417	0.463	0.387	0.484	0.449	0.487	0.649	**0.660**

Table 1. Classification accuracies of various methods. **Bold** indicates best result(s), *italic* indicates that the given experiments were used for training.

Factor analysis of spatial movement paths

In the previous section, the proposed modeling framework was shown to give unequalled accuracy of modeling the time series data for acceleration. In this section we use the warping functions obtained to analyze the spatial movement paths and their dependence on task conditions. Temporal alignment of the spatial positions along the path for different repetitions and participants is necessary to avoid spurious spatial variance of the paths. The natural alignment of two movement paths is the one that matches their acceleration signatures. In other words, spatial positions along the paths at which similar accelerations are experienced should correspond to the same times. Thus, each individual spatial trajectory was aligned using the time warping predicted from the TMS_p-results of the previous section. Every sample path was represented by 30 equidistant sample points in time at which values were obtained by fitting a three-dimensional B-splines with 10 equidistantly spaced knots to each trajectory.

As an exemplary study, we analyze how spatial paths depend on obstacle height. We do this separately for each distance, so that we perform five separate analyses, one for each obstacle placement. In each analysis we have 10 participants with 10 repetitions for each of 3 obstacle heights. The three-dimensional spatial positions along the movement path, $\boldsymbol{y}_{ijh} \in \mathbb{R}^{30\times 3}$, depend on participant $i = 1, \ldots, 10$, repetition $j = 1, \ldots, 10$ and height $h = 1, 2, 3$.

We are interested in understanding how the space-time structure of movement captured the 30 by 3 dimensions of the trajectories, $\boldsymbol{y}_{ijh}$, varies when obstacle height is varied. We the seek to find a low-dimensional affine subspace of the space-time representation of the movements within which movements vary, once properly aligned. That subspace provides a low-dimensional model of movement paths on the basis of which we can analyze the data.

We identify the low-dimensional subspace based on a novel factor analysis model. In analogy to principal component analysis (PCA), q so-called *loadings* are estimated that represent dominant patterns of variation along movement trajectories. In contrast to PCA, the factor analysis model does not only model the residual-variance of independent paths around the mean, but also allows one to include covariates from the experimental design, for example by taking the repetition structure of participants and systematic effects of obstacle height into account. In other words, the proposed factor analysis model is a generalization of PCA suitable for addressing the question at hand while obeying the study design.

The idea is to use the mean movement trajectory, $\boldsymbol{\theta} \in \mathbb{R}^{30\times 3}$, of one condition, the lowest obstacle height, as a reference. The movement trajectories $\boldsymbol{y}_{ijh}$ (30 time steps and 3 cartesian coordinates; participant i; repetition j, and experimental condition with height h) are then represented through their deviation from the reference path. We estimate the hypothesized low-dimensional affine subspace in which these deviations lie. That subspace is spanned by the q orthonormal (30×3)-dimensional columns of the loadings matrix $W \in \mathbb{R}^{(30\times 3)\times q}$. We assume a mixed-effect structure on the weights for the loadings that takes into account both the categorical effect of obstacle-height and random effects of

participant and repetition. This amounts to a statistical model

$$\boldsymbol{y}_{ijh} = \boldsymbol{\theta} + (X_h\boldsymbol{\beta} + \sum_{l=1}^{3} Z_{i,g_l(j,h),l})W^\top + \boldsymbol{\varepsilon}_{ij}, \tag{5}$$

where $X_h \in \mathbb{R}^{1\times 2}$ represents the covariate design that indicates obstacle heights: S: $X_1 = (0,0)$; M: $X_2 = (1,0)$; and T: $X_3 = (0,1)$. The parameters, $\boldsymbol{\beta} \in \mathbb{R}^{2\times q}$, are the weights for the loadings that account for the systematic deviation of obstacle heights, M and T from the reference height, S. g_l is the factor that describes the lth level random effects design (participant, participants' reaction to obstacle-height change, and repetition). $Z_{i,g_l(j,h),l} \in \mathbb{R}^{1\times q}$ are independent latent Gaussian variables with zero-mean and a covariance structure modeled with three $q \times q$ covariance matrices, each describing the covariance between loadings within a level of the random-effect design. $\boldsymbol{\varepsilon}_{ij} \in \mathbb{R}^{30\times 3}$ is zero-mean Gaussian noise with diagonal covariance matrix Λ with one variance parameter per dimension.

The loading matrix W is identifiable in a similar way as for usual PCA. Firstly, the scaling of W is identified by the assumption that $W^\top W$ is the q-dimensional identity matrix. Secondly, the rotation of W is identified by the assumption that the total variance of the latent variables for a single curve

$$\sum_{l=1}^{3} \mathrm{Var}(Z_{i,g_l(j,h),l}),$$

is a diagonal matrix. This identifies the loading matrix W with probability 1.

The models were fitted using maximum likelihood estimation by using an ECM algorithm [52] that had been accelerated using the SQUAREM method [53].

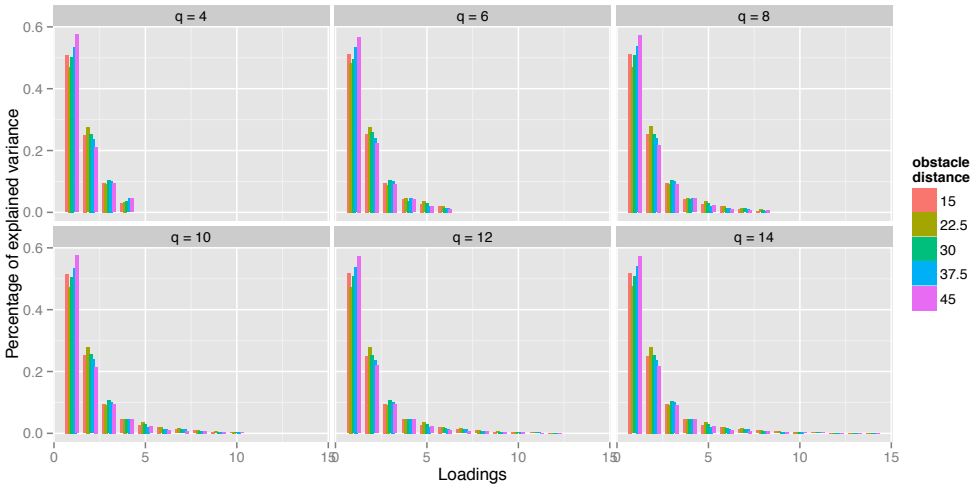

Figure 9. Percentage of variance explained by individual loadings under different total number of loadings q and obstacle distance.

Figure 9 shows the percentage of explained variance for various values of q across different obstacle distances. For $q > 8$, the average percentage of variance explained by the ninth loading ranges from 1% to 2% and the combined percentage of variance explained by the loadings beyond number eight remains under 3%. From this perspective, $q = 8$ seems like a reasonable choice, with the loadings explaining 97.1% of the variance, meaning that the error term $\boldsymbol{\varepsilon}_{ij}$ should account for the remaining 2.9%. In the following, all results are based on the model with $q = 8$.

Modeling obstacle height The fitted mean trajectories for the three different obstacle heights at distance $d = 30.0$ cm can be found in Figure 10. A striking feature of the mean

paths is the apparent linear scaling of elevation, but also of the lateral excursion with height. (The difference in the frontal plane, not shown, was very small, but follows a similar pattern.) This leads to the hypothesis that the scaling of the mean trajectory with obstacle height can be described by a one-parameter regression model in height increase ($X_1 = 0$, $X_2 = 7.5$, $X_3 = 15$) rather than a more generic two-parameter ANOVA model.

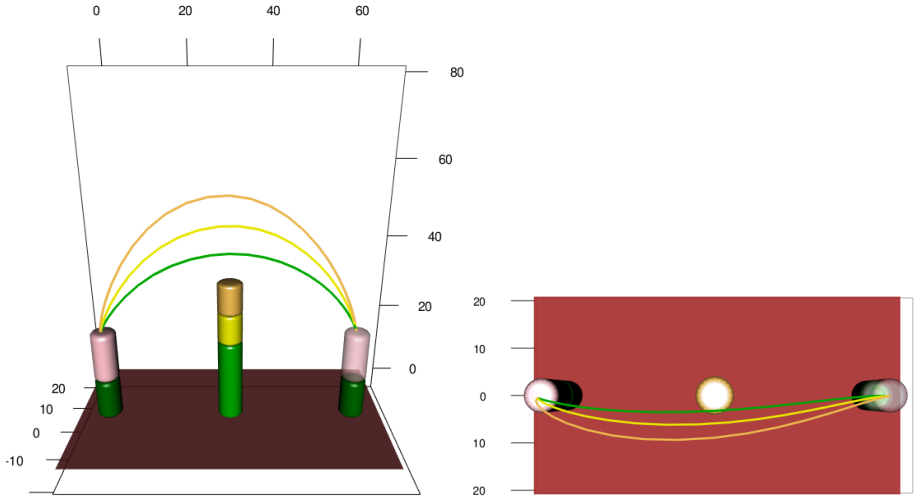

Figure 10. Mean paths for the three obstacle heights (green: small; yellow: middle, orange: tall) at obstacle distance $d = 30.0$ cm.

We fitted both models for every obstacle distance and performed likelihood-ratio tests. The p-values can be found in Table 2. They were obtained by evaluating twice the difference in log likelihood for the two models using a χ^2-distribution at $q = 8$ degrees of freedom. We see that no p-values are significant, so there is no significant loss in the descriptive power of the linear scaling model compared to the ANOVA model. The remaining results in the paper are all based on the model with a regression design.

Table 2. p-values for the hypothesis of linearly amplified path changes in obstacle height increase factor.

Obstacle distance	15.0 cm	22.5 cm	30.0 cm	37.5 cm	45.0 cm
p-value	0.478	0.573	0.093	0.764	0.362

Discovering the time-structure of variance along movement trajectory A strength of our approach to time warping is that we can estimate variability more reliably. In addition to observation noise, we model three sources of variation in the observed movement trajectories: individual differences in the trajectory, individual differences caused by changing obstacle height, and variation from repetition to repetition. The variances described from these three sources are independent of obstacle height. In figures 11 and 12, two spatial representations of the mean movement path for the medium obstacle height are shown. The five distances of the obstacle from the starting position are shown in the five rows of the figures. The three columns show variance originating from individual differences in the trajectory, individual differences caused by changing obstacle height, and variation from repetition to repetition (from left to right). Variance is illustrated at eight equidistant points in time along the mean path by ellipsoids that mark 95% prediction for each level of variation.

Note the asymmetry of the movements with respect to obstacle position, both in terms of path and variation. This asymmetry reflects the direction of the movement. Generally, variability is higher in the middle of the movement than early and late in the movement. Individual differences caused by change in obstacle height (middle column) are small and lie primarily along the path. That is, individuals adapt the timing of the movement differently as height is varied. Individual differences in the movement path itself (left

column) are largely differences in movement parameters: individuals differ in the maximal elevation and in the lateral positioning of their paths, not as much in the time structure of the movements. Variance from trial to trial (right column) is more evenly distributed, but is largest along the path reflecting variation in timing.

These descriptions are corroborated by the comparisons of the amounts of variance explained by the three effects in Figure 13. The obstacle distance of 45, in which the obstacle is close to the target lead to the largest variance in movement trajectory, with most of the increase over other conditions coming from repetition and individual differences caused by change in obstacle height. This suggests that this experimental condition is more difficult than the others, and perhaps much more so for the tall obstacle than for the small one. Apart from this condition, we see that the largest source of variation are individual differences in movement trajectory. The second largest source of variation was repetition. Individual differences caused by change in obstacle height were systematically the smallest source of variance.

Trajectory focal points A final demonstration of the strength of the method of analysis is illustrated in Figure 14, which shows the mean paths for all obstacle distances and all obstacle heights. For each obstacle height, the paths from different obstacle distances intersect both in the frontal and the vertical plane. These focal points occur approximately at the same distance along the imagined line connecting start and end position. This pattern is clearly visible in the front view of the mean trajectories in Figure 14. Due to the limited variation of the path in the horizontal plane (Figure 14 top view), this effect is less clear in the horizontal plane. This pattern may reflect a scaling law, a form of invariance of an underlying path generation mechanism.

Discussion

We have proposed a statistical framework for the modeling of human movement data. The hierarchical nonlinear mixed-effects model systematically decomposes movements into a common effect that reflects the variation of movement variables with time during the movement, individual effects, that reflect individual differences, variation from trial to trial, as well as measurement noise. The model amounts to a nonlinear time-warping approach that treats all sources of variances simultaneously.

We have outlined a method for performing maximum likelihood estimation of the model parameters, and demonstrated the approach by analyzing a set of human movement data on the basis of acceleration profiles in arm movements with obstacle avoidance. The quality of the estimates was evaluated in a classification task, in which our model was better able to determine if a sample movement came from a particular participant compared to state-of-the-art template-based curve classification methods. These results indicate that the templates that emerge from our nonlinear warping procedure are both more consistent and richer in detail.

We used the nonlinear time warping obtained from the acceleration profiles to analyze the spatial movement trajectories and their dependence on task conditions, here the dependence on obstacle height and obstacle placement along the path. We discovered that the warped movement path scales linearly with increasing obstacle height. Furthermore, we separated the variation around the mean paths into three levels: individual differences of movement trajectory, individual differences caused by change in obstacle height, and trial to trial variability. This combination of models uncovered clear and coherent patterns in the structure of variance. Individual differences in trajectory and variance from trial to trial were the largest sources of variance, with individual differences being primarily at the level of movement parameters such as elevation and lateral extent of the movement while variance from trial to trial contained a larger amount of timing variance. We documented a remarkable property of the movement paths when obstacle distance along the path is varied at fixed obstacle height: all paths intersect at a single point in space.

We believe that the approach we describe enhances the power of time series analysis as demonstrated in human movement data. The nonlinear time warping procedure makes

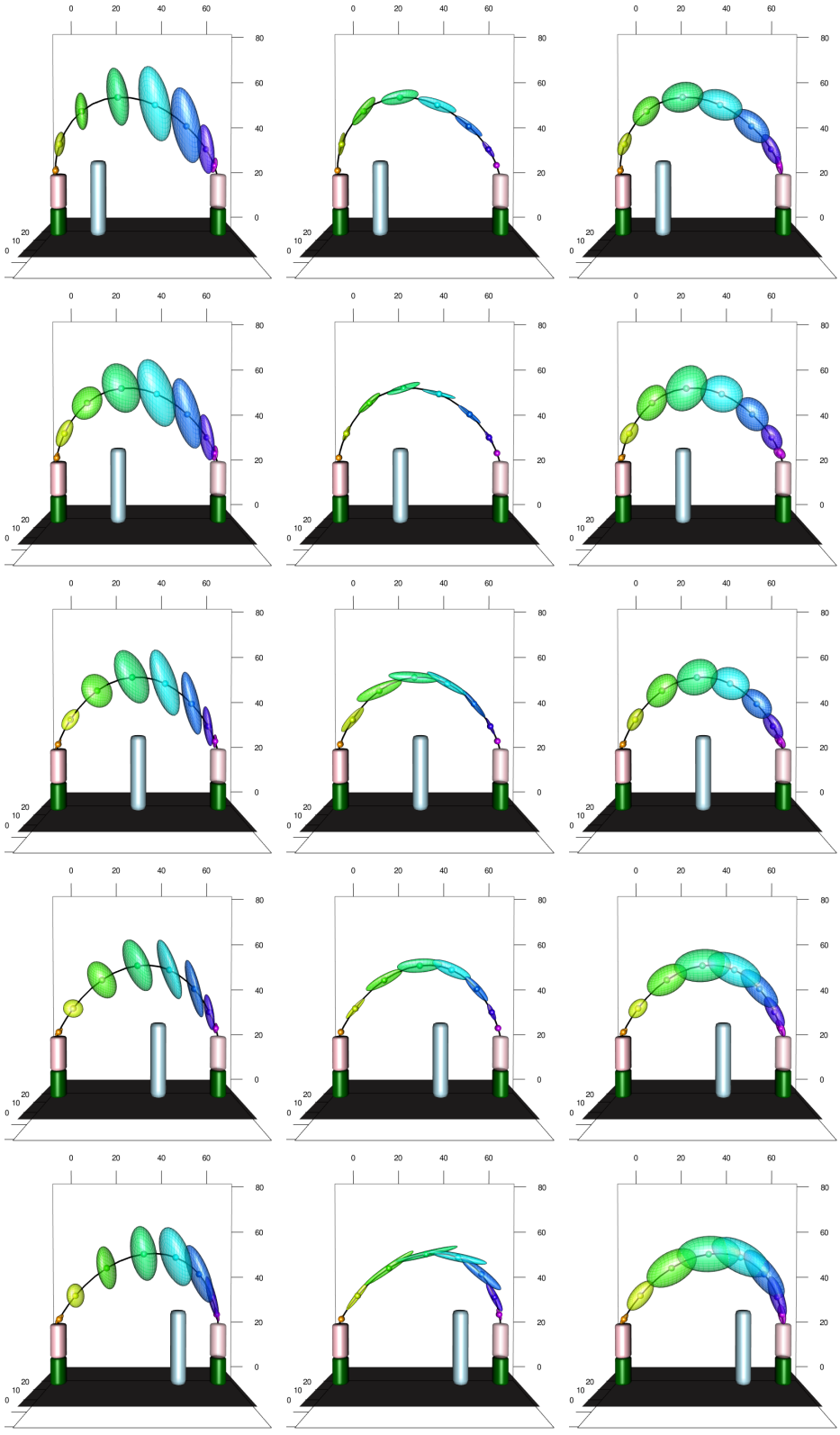

Figure 11. Illustration of the experimental setup for the medium height obstacle at all obstacle distances (rows) with the mean trajectory plotted. Along the trajectory eight equidistant points (in percentual warped time) are marked, and at each point 95% prediction ellipsoids are drawn. The three columns represent the random effects tied to participant, subjective reaction to height change and repetition, respectively.

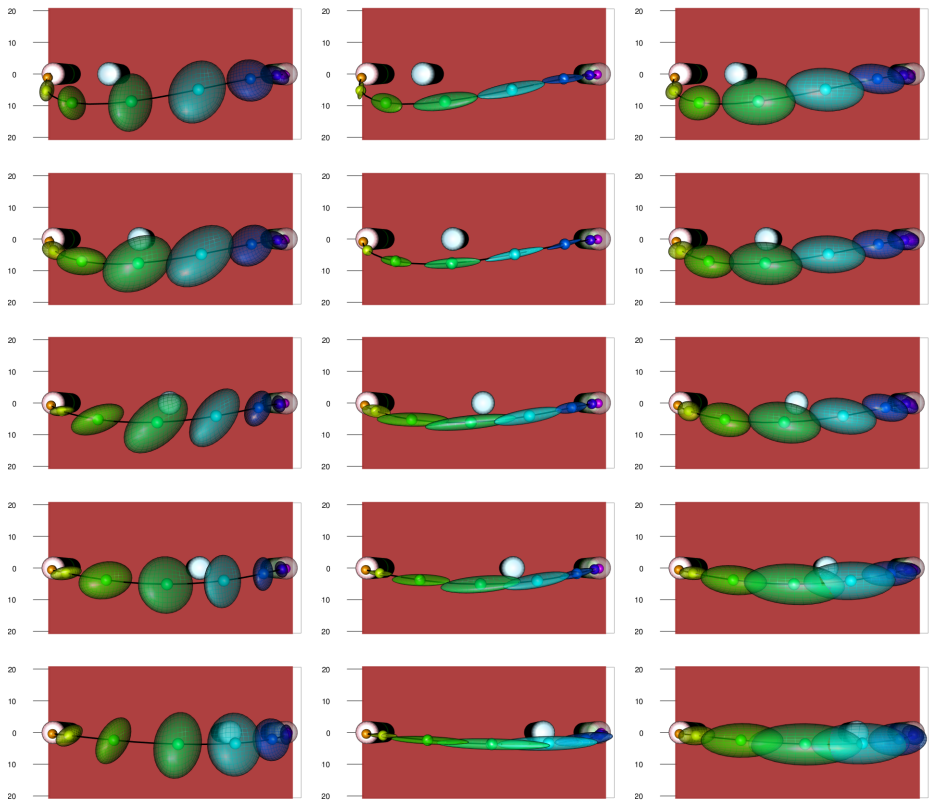

Figure 12. Top-view of the experimental setup from the top for the medium height obstacle at all obstacle distances with the mean trajectory plotted. Along the trajectory eight equidistant points (in percentual warped time) are marked, and at each point 95% prediction ellipsoids are drawn. The ordering is the same as in Figure 11.

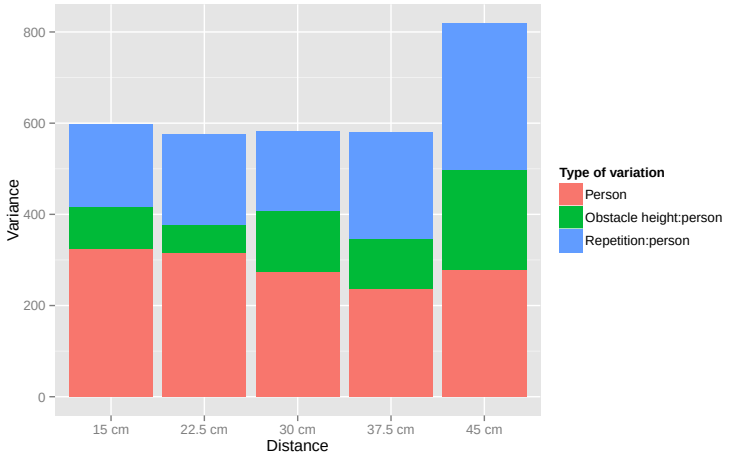

Figure 13. Amount of variance explained by random effects.

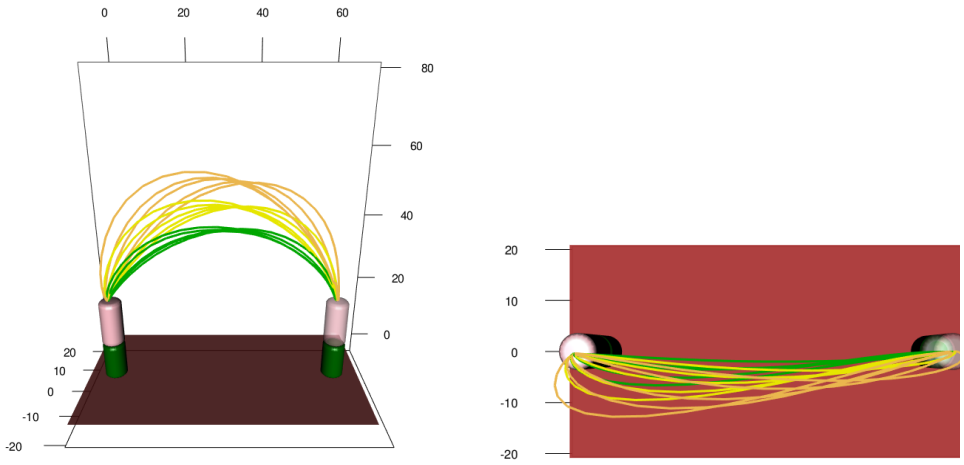

Figure 14. Front and top view of the mean trajectories for the 15 obstacle avoidance setups. Green lines correspond to low obstacles, yellow to medium obstacles and orange to tall obstacles.

it possible to obtain reliable estimates of variance along the movement trajectories and is strong in extracting individual differences. This advantage can be leveraged by combining the nonlinear time warping with factor analysis to extract systematic dependencies of movements on task conditions at the same time as tracking individual differences, both base-line and with respect to the dependence on task conditions, as well as variance across repetitions of the movement.

Recent theoretical accounts have used the analysis of variance across repetitions of movements to uncover coordination among the many degrees of freedom of human movement systems [17]. Differences in variance between the subspace that keeps hypothesized relevant task variables invariant and the subspace within which such task variables vary support hypotheses about the task-dependent structure of the underlying control systems. Because variance is modulated in time differently across the two subspaces, a more principled decomposition of time dependence and variance from trial to trial would give such analyses new strength. Because this application requires the extension of the proposed method to multivariate time series, it is beyond the scope of this paper. Together with the considerable practical interest in identifying individual differences, these theoretical developments underscore that the method proposed here is timely and worth the methodological investment.

Supporting Information

A primer on model building for movement data

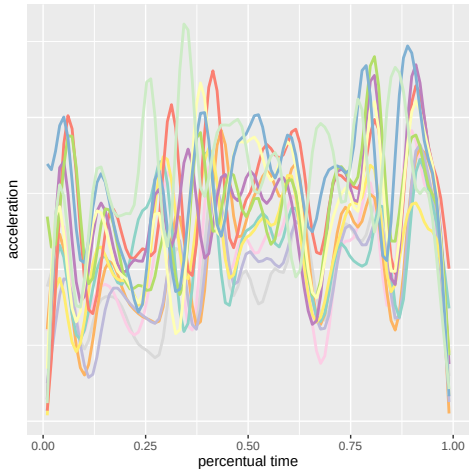

Figure 15. Twelve acceleration functions corresponding to repetitions of a signature being written.

The two major types of variation in movement data are path variation (amplitude) and movement timing variation (time warping). From a statistical modeling perspective, it is natural to model these effects as realizations of random processes across repetitions of the task at hand, since this allows a data driven regularization of the predictions of these effects. We consider the class of models on the form

$$y_i(t_k) = \theta(v(t_k, \boldsymbol{w}_i)) + x_i(t_k) + \varepsilon_{ik} \tag{6}$$

where θ is the mean profile, v is a warping function that depends on the random warping parameters $\boldsymbol{w}_i \in \mathbb{R}^{n_w}$ that are assumed to be independent across i and multivariate zero-mean Gaussian with covariance matrix $\sigma^2 C$, the x_i terms are independent zero-mean Gaussian process with covariance function $\sigma^2 \mathcal{S}$, and the ε_{ik}-terms are independent zero-mean Gaussian noise with variance σ^2.

To use model (6) we need to choose the type of mean function θ, the type of warping function v as well as the covariance structures for $\boldsymbol{w}_i$ and x_i. Below is a list of considerations of how to do these model choices based on the experiment at hand.

θ: A good allround choice is to model θ as a B-spline using a functional basis. For periodic movement sequences, a Fourier basis may sometimes be preferred. To choose the number of basis functions to use we need to consider the data at hand. For experiments with dense sampling and a clear systematic pattern in the trajectories the number of basis functions should be just be sufficiently high to model the mean pattern. If on the other hand the trajectories are sparsely observed in time or the common pattern is very unclear, one should choose a small number of basis functions to avoid local overfitting.

v: The behavior of the warping function should be driven by the random variables $\boldsymbol{w}_i$. We will consider warping functions where $\boldsymbol{w}_i$ models disparities from the identity mapping (corresponding to no warp), and v is an interpolating function of these random disparities at a set of specified anchor points $\boldsymbol{t}^w \in \mathbb{R}^{n_w}$. If one needs to predict derivatives such as velocity or acceleration of the observed profiles the interpolation should be smooth (e.g. a cubic spline). If no derivatives are needed, one should prefer simpler models such as linear interpolation as this reduces the nonlinear contribution of the derivative term in the linearization term Z and thus reduces the complexity the estimation problem, see model (3).

C: The covariance matrix of the random disparities $\boldsymbol{w}_i$ should be chosen to respect the experimental setup. If movements are modeled in percentual time, and the beginning and end of the observed trajectories correspond to the same states across movement (e.g. beginning and end of movement), the model for $\boldsymbol{w}_i$ should respect that. The simplest such model is to assume that $\boldsymbol{w}_i$ is a Brownian bridge observed at the discrete anchor points $\boldsymbol{t}^w$. For other types of data one may wish to include a random Gaussian time shift (add constant matrix to the covariance of the non-shift part of the model) or have an open end point which could be modeled using a Brownian motion model. If n_w is low relative to the number of repetitions one may model C as a completely free covariance matrix.

$\mathcal{S}$: A good allround choice for the covariance function of the amplitude variance is the Matérn covariance function. The Matérn covariance has three parameters, scale, range and smoothness. The scale parameter determines the variance of the process, the range parameter determines the strength of the correlation over time and the smoothness parameter determines the smoothness of the corresponding process. If one wants to simplify the optimization problem, one may fix the smoothness parameter at some value that represents sufficient smoothness, for example 2 corresponding to twice differentiable sample paths of the amplitude effect. For experiments with fixed start and end values one may use a bridge process such as the Brownian bridge, however, it is often preferable to use a less specific model than an overly specific model. For additive effects such as x_i, even slight misspecification of a bridge covariance structure at the beginning and end of movement (where variance and covariance go from zero to non-zero) may result in considerable bias of the corresponding parameters.

Consider the handwriting signature data in percentual time in Figure 15. The data consist of 12 acceleration magnitude profiles, each with 98 observations, corresponding to repetitions of a signature being written by a participant. This data has previously been used as an example in [54]. A reproducible pattern across repetitions is in the nature of the task, and we also see a strong consistent pattern across the samples, but the curves are both misaligned and vary systematically in amplitude. Using the considerations above, we choose a B-spline basis with 40 interior knots to have sufficient flexibility to model the mean, we choose v to be a piecewise linear interpolation of the disparities $\boldsymbol{w}_i$ that we model as discretely observed Brownian bridges over $n_w = 20$ equidistant anchor points. For the amplitude covariance $\mathcal{S}$ we choose a Matérn covariance with unknown scale, range and smoothness.

The alignment of the proposed model is displayed in Figure 16. We see a neat alignment of the samples and a mean function that represents the mean pattern well, with no indications of local overfitting. Similarly for the warping functions, we only see small systematic deviations from the identity warp, despite of the high number of anchor points. The maximum likelihood estimates for the variance parameters were as follows: the warp scale estimate was 14.1, the variance scale estimate for the amplitude effect was 54.4, the range parameter estimate was $8.2 \cdot 10^{-3}$, the smoothness parameter was 6.2, and the noise variance σ^2 was estimated to be $1.4 \cdot 10^{-4}$. This suggests that the systematic part of the amplitude variation explains more than 99.9% of the amplitude variation, which fits well with the smooth functional samples.

To find the best among multiple models, one can compare different models using cross-vaildation, as was done in this paper, if such a setup is meaningful for the application at hand. In general one can do model selection based on the corrected conditional AIC of the linearized likelihoods [55].

R code for fitting the model to the signature data

Suppose that `y` is a list containing the 12 acceleration trajectories and `t` is a list of the corresponding observation times. The model described above can be specified and fitted using the code given below. The methods in the `pavpop` R package are thoroughly documented with a wide array of examples in the package help pages and vignettes.

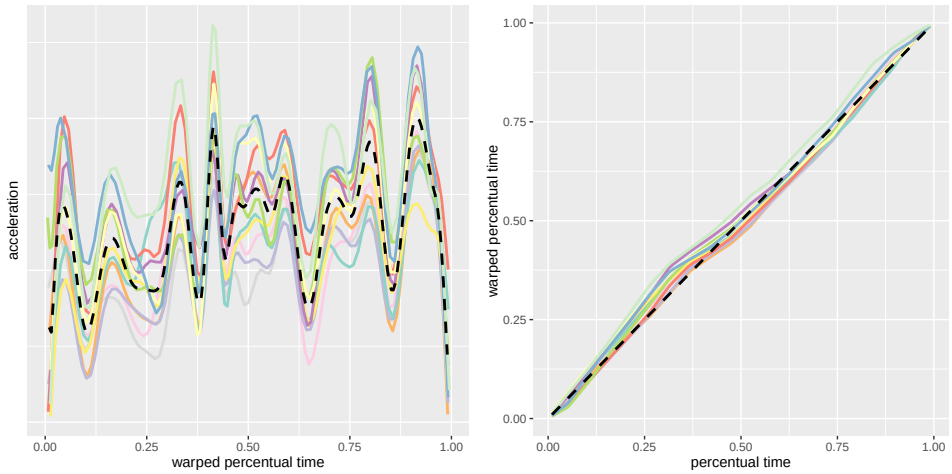

(a) Aligned samples and mean (dashed)

(b) Warping functions compared to the identity (dashed)

Figure 16. The aligned acceleration functions from Figure 15 (a), along with the predicted warping functions (b).

```
# Install and load pavpop R package
if (packageVersion("devtools") < 1.6) {
  install.packages("devtools")
}
devtools::install_github('larslau/pavpop')
library(pavpop)

# Set up basis function
kts <- seq(0, 1, length = 42)[2:41]
basis_fct <- make_basis_fct(kts = kts, intercept = TRUE,
                            control = list(boundary = c(0, 1)))

# Set up warp function
tw <- seq(0, 1, length = 20)
warp_fct <- make_warp_fct('piecewise-linear', tw)

# Set up covariance functions and roughly initialize parameters
warp_cov_par <- c(tau = 10)
warp_cov <- make_cov_fct(Brownian, noise = FALSE, param = warp_cov_par,
                         type = 'bridge')

amp_cov_par <- c(scale = 4, range = 1, smoothness = 2)
amp_cov <- make_cov_fct(Matern, noise = TRUE, param = amp_cov_par)

#
# Estimate in the model
#

# Rough bounds on parameters
lower <- c(1e-3, 1e-3, 1e-3, 1e-3)
upper <- c(1000, 10, 10, 10)

res <- pavpop(y, t, basis_fct, warp_fct, amp_cov, warp_cov,
              iter = c(5, 20), homeomorphism = 'soft',
```

```
                like_optim_control = list(lower = lower, upper = upper))
```

Simulation study

To evaluate the proposed algorithm for maximum likelihood estimation, we simulated data from the proposed model under the maximum likelihood estimates on the full data using a sampling setup identical to the central experiment ($d = 30.0$ cm, medium obstacle). We simulated 1000 outcomes and ran the estimation procedure as described in the section on modeling of effects and the algorithmic approach. The total runtime of the 1000 estimation procedures was approximately 6 hours on a 64-core machine.

The densities of the integrated square estimation errors (L^2 error) for the estimated mean profiles (experiment and participant) are shown in the right panel of Figure 17. For comparison, the experiment-specific and participant mean profiles have been estimated using ordinary least squares (OLS) estimation with the correctly specified spline model for the mean. The corresponding densities are shown in the left panel. We note that the densities are shown on squareroot scale to enable visual inspection of the differences. We see that the estimate for the experiment-specific mean profile is marginally more stable for the OLS estimation, but results are close-to perfect for both methods. For the participant-specific effects, however, we see that the proposed model that aligns samples within participant using a random warping function gives L^2 errors that are approximately an order of magnitude lower than simple OLS estimation.

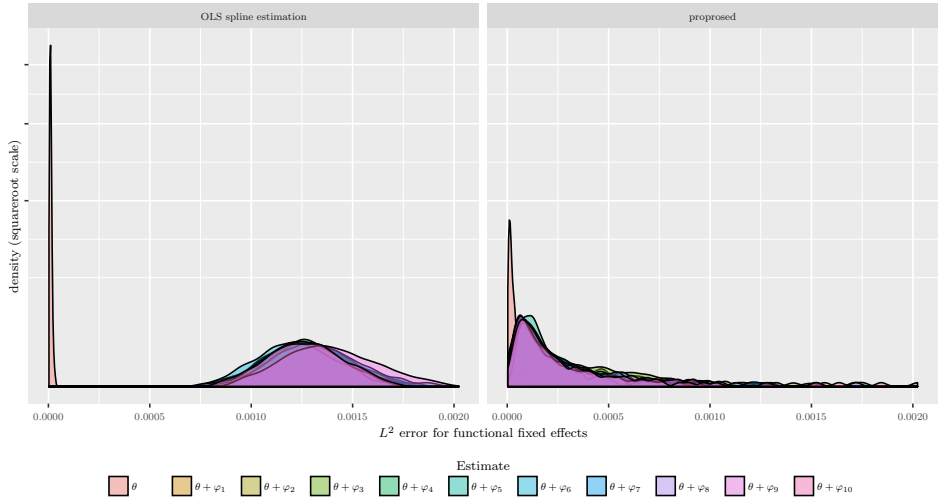

Figure 17. Densities of the integrated square estimation errors (L^2 errors) for the common and participant-specific mean functions in the simulation study. The left panel shows results for ordinary least square (OLS) estimation and the right panel shows the results for the proposed model and estimation algorithm. Both models were fitted using the correctly specified spline model for the mean. Note that the density is displayed on squareroot scale.

Figure 18 displays densities of the differences between the maximum likelihood estimates for the true participant-specific warping parameters across participants. The estimates generally seem unbiased with small variance around the true warping parameters.

Figure 19 displays densities for the parameter estimates in the simulated experimental setups. We see that the estimators for the noise scale σ and the scales for the warp parameters $\sigma\gamma$ both seem to have a small upward bias. The scale $\sigma\tau$ of the serially correlated effects and the range parameter $1/\alpha$ both seem to be estimated with very little or no bias. Slightly biased variance-parameter estimates are to be expected in likelihood-based inference [56], in particular in nonlinear models where bias-reducing estimation methods such as restricted maximum likelihood (REML), that are inherently linear, are not available.

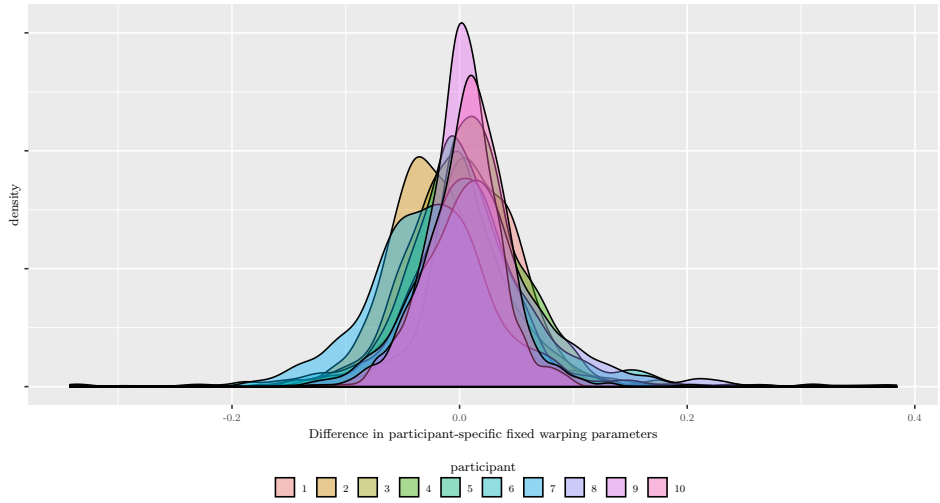

Figure 18. Densities of the difference between the estimated and the true participant-specific warping parameters across participants.

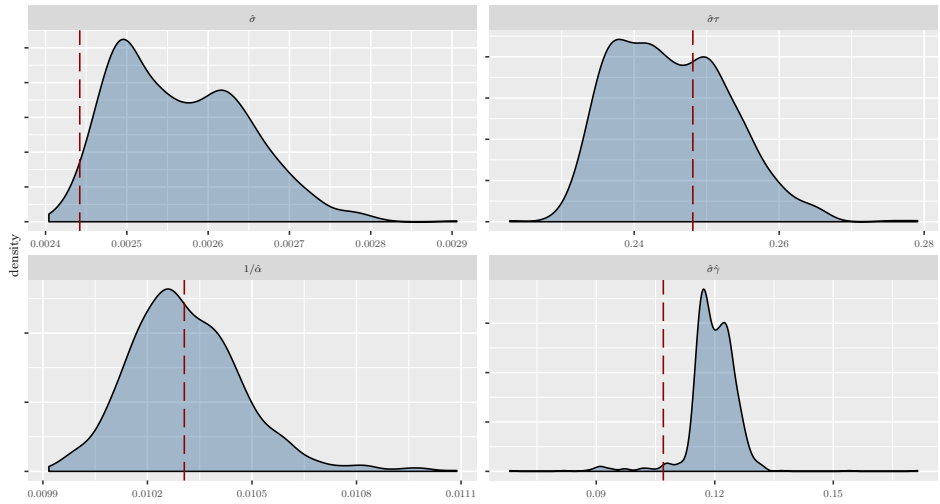

Figure 19. Densities of the estimated variance parameters in the simulated experimental setups. Dashed red lines indicate the true values of the parameters.

Cross-validation grids for motion classification

Cross-validation was done over:

MBM number of bands J in $\{1, 2, 3, 4, 5, 6\}$.
DTW degrees of freedom for B-spline basis $\{8, 13, 18, 23, 28, 33, 38\}$. For DTW_p $\{8, 9, \ldots, 18\}$.
FR number of principal components in $\{1, 2, 3, 4, 5\}$.
FR_E number of principal components in $\{1, 2, 3, 4, 5\}$ and weighting between phase and amplitude distance in $\{0.0, 0.5, \ldots, 5.0\}$.

References

[1] Morasso P. Three dimensional arm trajectories. Biological Cybernetics. 1983;48(3):187–194.
[2] Soechting JF, Terzuolo CA. Organization of arm movements in three-dimensional space. Wrist motion is piecewise planar. Neuroscience. 1987;23(1):53–61.

[3] Morasso P. Spatial control of arm movements. Experimental Brain Research. 1981;42(2):223–227.
[4] Lacquaniti F, Terzuolo C, Viviani P. The law relating the kinematic and figural aspects of drawing movements. Acta psychologica. 1983;54(1):115–130.
[5] Viviani P, McCollum G. The relation between linear extent and velocity in drawing movements. Neuroscience. 1983;10(1):211–218.
[6] Bennequin D, Fuchs R, Berthoz A, Flash T. Movement timing and invariance arise from several geometries. PLoS Computational Biology. 2009;5(7):e1000426.
[7] Erlhagen W, Schöner G. Dynamic field theory of movement preparation. Psychological Review. 2002;109(3):545–572.
[8] Georgopoulos AP. Current issues in directional motor control. Trends in Neurosciences. 1995;18:506–510.
[9] Schwartz AB. Useful signals from motor cortex. The Journal of Physiology. 2007;579(3):581–601.
[10] Harpaz NK, Flash T, Dinstein I. Scale-invariant movement encoding in the human motor system. Neuron. 2014;81(2):452–462.
[11] Zhang W, Rosenbaum DA. Planning for manual positioning: the end-state comfort effect for manual abduction–adduction. Experimental Brain Research. 2008;184(3):383–389.
[12] Cutting JE, Kozlowski LT. Recognizing friends by their walk: Gait perception without familiarity cues. Society, Bulleting of the Psychonomic. 1977;9(5):353–356.
[13] Pollick FE, Kay JW, Heim K, Stringer R. Gender recognition from point-light walkers. Journal of Experimental Psychology: Human Perception and Performance. 2005;31(6):1247.
[14] Lu J, Wang G, Moulin P. Human identity and gender recognition from gait sequences with arbitrary walking directions. Information Forensics and Security, IEEE Transactions on. 2014;9(1):51–61.
[15] Schöner G, Kelso JAS. Dynamic pattern generation in behavioral and neural systems. Science. 1988;239:1513–1520.
[16] Scholz JP, Schöner G. The Uncontrolled Manifold Concept: Identifying Control Variables for a Functional Task. Experimental Brain Research. 1999;126:289–306.
[17] Latash ML, Scholz JP, Schöner G. Toward a new theory of motor synergies. Motor Control. 2007;11:276–308.
[18] Ramsay JO, Silverman BW. Functional Data Analysis. 2nd ed. Springer; 2005.
[19] Pinheiro JC, Bates DM. Mixed effects models in S and S-PLUS. Springer; 2000.
[20] Lindstrom MJ, Bates DM. Nonlinear Mixed Effects Models for Repeated Measures Data. Biometrics. 1990;46(3):673–687.
[21] Grimme B, Lipinski J, Schöner G. Naturalistic arm movements during obstacle avoidance in 3D and the identification of movement primitives. Experimental Brain Research. 2012;222(3):185–200.
[22] Raket LL. pavpop version 0.10; 2016. Available from: https://github.com/larslau/pavpop/.
[23] Grimme B. Analysis and identification of elementary invariants as building blocks of human arm movements. International Graduate School of Biosciences, Ruhr-Universität Bochum; 2014. (In German).
[24] Sakoe H, Chiba S. Dynamic programming algorithm optimization for spoken word recognition. Acoustics, Speech and Signal Processing, IEEE Transactions on. 1978;26(1):43–49.
[25] Bruderlin A, Williams L. Motion signal processing. In: Proceedings of the 22nd annual conference on Computer graphics and interactive techniques. ACM; 1995. p. 97–104.
[26] Troje NF. Decomposing biological motion: A framework for analysis and synthesis of human gait patterns. Journal of Vision. 2002;2(5):371–387.
[27] Berndt DJ, Clifford J. Using Dynamic Time Warping to Find Patterns in Time Series. In: KDD workshop. vol. 10. Seattle, WA; 1994. p. 359–370.
[28] Gavrila D, Davis L, et al. Towards 3-D model-based tracking and recognition of human

movement: a multi-view approach. In: In International Workshop on Automatic Face- and Gesture-Recognition. IEEE Computer Society; 1995. p. 272–277.
[29] Giese MA, Poggio T. Morphable models for the analysis and synthesis of complex motion patterns. International Journal of Computer Vision. 2000;38(1):59–73.
[30] Niennattrakul V, Ratanamahatana CA. Inaccuracies of shape averaging method using dynamic time warping for time series data. In: Computational Science–ICCS 2007. Springer; 2007. p. 513–520.
[31] Petitjean F, Ketterlin A, Gançarski P. A global averaging method for dynamic time warping, with applications to clustering. Pattern Recognition. 2011;44(3):678–693.
[32] Rønn BB. Nonparametric maximum likelihood estimation for shifted curves. Journal of the Royal Statistical Society: Series B (Statistical Methodology). 2001;63(2):243–259.
[33] Gervini D, Gasser T. Nonparametric maximum likelihood estimation of the structural mean of a sample of curves. Biometrika. 2005;92(4):801–820.
[34] Rønn BB, Skovgaard IM. Nonparametric maximum likelihood estimation of randomly time-transformed curves. Brazilian Journal of Probability and Statistics. 2009;23(1):1–17.
[35] Beath KJ. Infant growth modelling using a shape invariant model with random effects. Statistics in medicine. 2007;26(12):2547–2564.
[36] Cole TJ, Donaldson MD, Ben-Shlomo Y. SITAR—a useful instrument for growth curve analysis. International Journal of Epidemiology. 2010;39:1558–1566.
[37] Raket LL, Sommer S, Markussen B. A nonlinear mixed-effects model for simultaneous smoothing and registration of functional data. Pattern Recognition Letters. 2014;38:1–7.
[38] Ilg W, Bakir G, Franz M, Giese M. Hierarchical spatio-temporal morphable models for representation of complex movements for imitation learning. In: Nunes U., de Almeida A., Bejczy A., Kosuge K., and Machado J., In Proceeding of The 11th International Conference on Advanced Robotics. vol. 2; 2003. p. 453–458.
[39] Marron JS, Ramsay JO, Sangalli LM, Srivastava A. Functional data analysis of amplitude and phase variation. Statistical Science. 2015;30(4):468–484.
[40] Wolfinger R. Laplace's approximation for nonlinear mixed models. Biometrika. 1993;80(4):791–795.
[41] Robinson GK. That BLUP is a Good Thing: The Estimation of Random Effects. Statistical Science. 1991;6(1):15–32.
[42] de Boor C. A Practical Guide to Splines. Revised ed. Springer-Verlag, Berlin; 2001.
[43] Billingsley P. Convergence of probability measures. vol. 493 of Wiley Series in Probability and Statistics. John Wiley & Sons; 1999.
[44] Flash T, Hogan N. The coordination of arm movements: an experimentally confirmed mathematical model. The Journal of Neuroscience. 1985;5(7):1688–1703.
[45] Stein ML. Interpolation of Spatial Data: Some Theory for Kriging. Springer; 1999.
[46] Arribas-Gil A, Romo J. Robust depth-based estimation in the time warping model. Biostatistics. 2012;13(3):398–414.
[47] Dimeglio C, Gallón S, Loubes JM, Maza E. A robust algorithm for template curve estimation based on manifold embedding. Computational Statistics & Data Analysis. 2014;70:373–386.
[48] Kurtek SA, Srivastava A, Wu W. Signal estimation under random time-warpings and nonlinear signal alignment. In: Advances in Neural Information Processing Systems; 2011. p. 675–683.
[49] Tucker JD. fdasrvf: Elastic Functional Data Analysis; 2014. R package version 1.4.2. Available from: http://CRAN.R-project.org/package=fdasrvf.
[50] Čencov NN. Statistical decision rules and optimal inference. American Mathematical Society; 2000.
[51] Tucker JD, Wu W, Srivastava A. Generative models for functional data using phase and amplitude separation. Computational Statistics & Data Analysis. 2013;61:50–66.
[52] Meng XL, Rubin DB. Maximum likelihood estimation via the ECM algorithm: A general framework. Biometrika. 1993;80(2):267–278.

[53] Varadhan R, Roland C. Simple and globally convergent methods for accelerating the convergence of any EM algorithm. Scandinavian Journal of Statistics. 2008;35(2):335–353.

[54] Srivastava A, Wu W, Kurtek S, Klassen E, Marron J. Registration of functional data using Fisher-Rao metric. arXiv preprint arXiv:11033817. 2011;.

[55] Greven S, Kneib T. On the behaviour of marginal and conditional AIC in linear mixed models. Biometrika. 2010;97(4):773–789.

[56] Harville DA. Maximum likelihood approaches to variance component estimation and to related problems. Journal of the American Statistical Association. 1977;72:320–340.